Astrocytic Glutamate Transport Regulates a *Drosophila* CNS Synapse That Lacks Astrocyte Ensheathment

Sarah E. MacNamee,[1]* Kendra E. Liu,[1] Stephan Gerhard,[2,3] Cathy T. Tran,[1] Richard D. Fetter,[2] Albert Cardona,[2] Leslie P. Tolbert,[1] and Lynne A. Oland[1]

[1]Department of Neuroscience, University of Arizona, Tucson, Arizona 85721
[2]HHMI Janelia Research Campus, Ashburn, Virginia 20147
[3]Institute of Neuroinformatics, University of Zurich and ETH Zurich, CH-8057 Zurich, Switzerland

ABSTRACT

Anatomical, molecular, and physiological interactions between astrocytes and neuronal synapses regulate information processing in the brain. The fruit fly *Drosophila melanogaster* has become a valuable experimental system for genetic manipulation of the nervous system and has enormous potential for elucidating mechanisms that mediate neuron–glia interactions. Here, we show the first electrophysiological recordings from *Drosophila* astrocytes and characterize their spatial and physiological relationship with particular synapses. Astrocyte intrinsic properties were found to be strongly analogous to those of vertebrate astrocytes, including a passive current-voltage relationship, low membrane resistance, high capacitance, and dye-coupling to local astrocytes. Responses to optogenetic stimulation of glutamatergic premotor neurons were correlated directly with anatomy using serial electron microscopy reconstructions of homologous identified neurons and surrounding astrocytic processes. Robust bidirectional communication was present: neuronal activation triggered astrocytic glutamate transport via excitatory amino acid transporter 1 (Eaat1), and blocking Eaat1 extended glutamatergic interneuron-evoked inhibitory postsynaptic currents in motor neurons. The neuronal synapses were always located within 1 μm of an astrocytic process, but none were ensheathed by those processes. Thus, fly astrocytes can modulate fast synaptic transmission via neurotransmitter transport within these anatomical parameters. J. Comp. Neurol. 524:1979–1998, 2016.

© 2016 Wiley Periodicals, Inc.

INDEXING TERMS: electrophysiology; optogenetics; electron microscopy; coupling; RRID: SCR_007353; RRID: AB_528235; RRID: AB_221477; RRID: AB_2313643; RRID: AB_528122; RRID: AB_2490070

The fruit fly *Drosophila melanogaster* offers sophisticated tools for genetic manipulation of the nervous system and has proven to be a robust and relevant system for elucidating neuronal function at the levels of genes, cellular physiology, and neuronal circuits (Venken et al., 2011). More recently, flies have become a valuable experimental system for identifying glial genes and signaling pathways that mediate neuron–glia interactions (Egger et al., 2002; Freeman et al., 2003; Altenhein et al., 2006; Coutinho-Budd and Freeman, 2013). One glial subtype has been of particular interest as a model for astrocyte development and function. These fly astrocyte-like glial cells have come to be called simply astrocytes; there are six astrocytes per hemisegment in the larval ventral nerve cord (VNC) (Stork et al., 2014).

© 2016 Wiley Periodicals, Inc.

Morphologically, the highly branched processes of fly astrocytes strongly resemble those of vertebrate protoplasmic astrocytes, and their presence throughout the

Grant sponsor: National Science Foundation; Grant number: IOS-1353739 (to L.A.O.) and Graduate Research Fellowship (to S.E.M.); Grant sponsor: the University of Arizona (to L.P.T.); Grant sponsor: HHMI Janelia (to A.C.); Swiss National Science Foundation; Grant number: 31003A_132969 (to A.C.); Grant sponsor: ARCS Foundation Phoenix Scholar Award (to S.E.M.); Grant sponsor: University of Arizona Gruener Travel Award (to S.E.M.); Grant sponsor: University of Arizona Neuroscience and Cognitive Science Summer Research Program (to K.E.L. and C.T.T.); Grant sponsor: Microscopy Society of America Undergraduate Research Scholarship (to K.E.L.).

*CORRESPONDENCE TO: Sarah E. MacNamee, Department of Neuroscience, University of Arizona, 1040 E. 4th St., GS Rm 611, Tucson, AZ 85721. E-mail: Smac3@email.arizona.edu

Received February 13, 2016; Revised April 8, 2016;
Accepted April 9, 2016.
DOI 10.1002/cne.24016
Published online April 25, 2016 in Wiley Online Library (wileyonlinelibrary.com)

synaptic neuropil suggests they may functionally regulate mature neuronal synapses (Awasaki et al., 2008). Molecular evidence indicates that fly astrocytes express neurotransmitter transporters (the glutamate transporter termed excitatory amino acid transporter 1, *Eaat1*, and γ-aminobutyric acid [GABA] transporter, *Gat*) (Rival et al., 2004; Thimgan et al., 2006) and receptors (metabotropic GABA receptors) (Mezler et al., 2001; Muthukumar et al., 2014), as well as gap-junction–forming innexins (Stebbings et al., 2002), much like their mammalian counterparts (Kimelberg and Nedergaard, 2010). Several complex behaviors have been shown to be influenced by genes expressed in *Drosophila* astrocytes. Larval locomotion rate is regulated by *Eaat1* (Stacey et al., 2010), courtship behavior is controlled by the amino acid transporter *genderblind* (Grosjean et al., 2008), and age-related memory impairment is sensitive to the pyruvate carboxylase *dPC* (Yamazaki et al., 2014). In addition, misexpression of the endocytosis mutant allele shi^{ts1} or the heat-activated cation channel *TrpA1* in astrocytes yields aberrant circadian locomotor rhythms (Ng et al., 2011) and olfactory processing (Liu et al., 2014), respectively. Each of these results provides indirect evidence that astrocytes modulate synapses in the fly, although they do not address which endogenously expressed astrocyte genes and proteins regulate synapses.

While anatomical and molecular features have been identified and a role in larval behavior has been demonstrated, the cellular physiology of *Drosophila* astrocytes has not been explored in any previous study, leaving basic questions about the anatomy and physiology of neuron–astrocyte interactions in the fly unanswered. Although there is a growing appreciation of heterogeneity within mammalian astrocyte populations (Matyash and Kettenmann, 2010; Oberheim et al., 2012), core electrophysiological features are shared across brain regions and have served as reliable identifiers of astrocytic cells. These features include a resting membrane potential that is more hyperpolarized than that of neuronal cells, a passive current-voltage relationship, and, for mature astrocytes examined *in vivo*, a lack of voltage-gated currents (Kafitz et al., 2008; Verkhratsky and Butt, 2013). Astrocyte electrical membrane responses to neuronal activity have been observed in rodent preparations and include potassium buffering currents (Meeks and Mennerick, 2007) as well as glutamate transport (Bergles and Jahr, 1997; Clark and Barbour, 1997; Lalo et al., 2006; Meeks and Mennerick, 2007; Zhang et al., 2009; Huda et al., 2013).

Viewed at high magnification, virtually all synaptic neuropils across species feature a feltwork of veil-like astrocytic processes that interdigitate between neuronal elements, such that no neuronal synapse operates at a great distance from an astrocytic process. Although astrocytic coverage of synapses has been examined in detail only in a few brain regions, at least in certain neuropils, astrocytic processes completely or partially enwrap synapses (Grosche et al., 1999; Xu-Friedman et al., 2001). However, the degree and nature of association between the two cell types vary, and the implications of these variations are poorly understood (Chao et al., 2002; Bernardinelli et al., 2014). Electron microscopic (EM) examination has revealed that fly synapses exhibit little astrocyte contact and no ensheathment (Stork et al., 2014; present study). The *Drosophila* neuropil is thus well suited to address questions about the spatial relationships needed to permit fast, physiological synapse–astrocyte interactions. This is critical, because although the notion that astrocytes are an essential third synaptic element (forming a "tripartite synapse") is well documented (Verkhratsky and Nedergaard, 2014), no prior study has directly linked the anatomical proximity of the astrocytic element to a given presynaptic element with functional, *in situ* recording. We asked whether *Drosophila* astrocytes and synapses form functional tripartite synapses, *i.e.*, whether perturbing astrocyte function can impact fast signal transmission, even in the absence of classical tripartite anatomy.

MATERIALS AND METHODS

Transgenic flies

The following stocks were obtained from the Bloomington Drosophila Stock Center (Indiana University, Bloomington, IN): UAS-CD4-tdGFP (Han et al., 2011), UAS-ChR2-H134R (Pulver et al., 2009), UAS-GFP.nls, LexAop2-CsChrimson, and GMR50G08-LexA (Pfeiffer et al., 2010), which was used to drive expression in looper interneurons. UAS-$dEaat1^{RNAi}$ flies (transformant ID 109401) were obtained from the Vienna Drosophila Resource Center (Vienna, Austria; Dietzl et al., 2007). The D42-GAL4 (Yeh et al., 1995) stocks used to drive expression in subsets of motor neurons, bipolar sensory neurons, and interneurons (Iyengar et al., 2011) were a gift from R.B. Levine (University of Arizona, Tucson, AZ). The alrm-GAL4 (Doherty et al., 2009) flies used to drive expression of green fluorescent protein (GFP) in *Drosophila* astrocytes were a gift from M. Freeman (University of Massachusetts Medical School, Worcester, MA). For D42>ChR2-H134R experiments, homozygous animals were used to achieve sufficient expression and subsequent depolarization to trigger neuronal action potentials. The remaining experimental animals used in this study were trans-heterozygous for GAL4/UAS insertions. Animals were reared on standard cornmeal-agar yeast fly food at 25°C on a 12-hour:12-hour

light:dark cycle, except for those expressing channelrhodopsins, which were raised on food containing 1 mM all-*trans*-retinal at 25°C in constant darkness.

Solutions

Extracellular recording saline was composed of: (in mM) 1.8 $CaCl_2$ (dihyd), 118 NaCl, 2 NaOH, 2 KCl (Thermo Fisher Scientific, Waltham, MA), 4 $MgCl_2$ (hexahyd), 25 sucrose, 5 trehalose, and 5 HEPES, and the pH was adjusted to 7.2 and osmolarity to 290 mOsm using sucrose (A solution: Jan and Jan, 1976). To reduce muscle contractions during dissection, $CaCl_2$ was replaced with $MgCl_2$ in the dissecting solution. To block calcium channels during physiological recordings, $CaCl_2$ was replaced with $MgCl_2$, and 1 mM $CdCl_2$ was also added. Intracellular recording saline included 5 KCl, 2 $MgCl_2$ (hexahyd), 2 EGTA, 20 HEPES, 133 K-gluconate, and 2 NaATP, and pH was adjusted to 7.4 using KOH, osmolarity to 290 mOsm using glucose. For some experiments, KCl was replaced with CsCl, and K-gluconate was replaced with CsOH and D-gluconic acid to block potassium channels. In some cases, Lucifer Yellow (2.7 mM), Alexa Fluor 568 (1 mM; Thermo Fisher Scientific, Waltham, MA), or Alexa Fluor 647 (1 mM) hydrazide was added to the pipette solution. Drugs were used at the following concentrations: tetrodotoxin (TTX; Calbiochem), 1 μM; tetraethylammonium (TEA), 50 mM; 4-aminopyridine (4-AP), 1.5 mM; DL-threo-β-benzyloxyaspartic acid (TBOA) (Tocris, Bristol, UK), 100 μM; picrotoxin (PTX), 100 μM. Unless otherwise specified, all reagents were from Sigma.

Whole-cell recordings

Wandering third-instar larvae were dissected in calcium-free A-solution (Jan and Jan, 1976). Central nervous systems were isolated, pinned in a Sylgard dish using pins made from 0.002-inch-diameter stainless steel wire, and continuously perfused with extracellular recording saline. Electrodes were pulled from thin-walled borosilicate glass capillaries (Fredrick and Dimmock, Millville, NJ; ID 0.9 mm OD 1.2 mm) using a Narishige PP-83 electrode puller, and were fire-polished to a resistance of 10–12 MΩ (astrocyte recordings) or 8–10 MΩ (motor neuron recordings). Preparations were visualized in the recording chamber using infrared and water-immersion optics. Recordings were made from astrocytes in the 2nd and 3rd thoracic segments (T2,3) or from the 1st abdominal segment (A1), where the space between the lateral and medial motor neuron clusters is larger, making the astrocyte cell bodies easier to identify than in the more posterior abdominal segments. Additionally, motor neuron physiology has been studied in these thoracic (Worrell and Levine, 2008) and upper abdominal (Baines and Bate, 1998) segments. All recordings were collected from one of the four astrocytes located on the dorsal surface of the neuropil of each hemisegment because the lateral and ventral astrocytes are too deep to access in whole-mount tissue. Focal protease application (Protease XIV, Sigma, St. Louis, MO) was used to expose the cells for recording. Enzyme (1–2 mg/mL) was delivered via gently broken recording electrodes, which also were used subsequently to remove overlying perineurial and subperineurial sheath-cell debris, following a widely used method to obtain motor neurons recordings in this preparation (Rhorbough and Broadie, 2002; Choi et al., 2004; Worrell and Levine, 2008; Pulver et al., 2009; Marley and Baines, 2011).

Signals were acquired with an Axopatch 200B amplifier (Molecular Devices, Sunnyvale, CA), filtered using a 1-kHz low-pass Bessel filter, digitized using a Digidata 1440A A-D converter (Molecular Devices), and collected at 10 kHz using pClamp 10 software (Molecular Devices). Leak subtraction was performed online using the pClamp P/4 opposite-polarity algorithm. In an effort to approximate the degree of error inherent in leak subtraction, manual *post hoc* leak subtraction was carried out by scaling the current responses to +10-mV and −10-mV steps proportionally to the voltage-step in question and performing subtraction (e.g., 2× the +10-mV step would be subtracted from the +20-mV step, 3× for a +30-mV step, etc.). Notably, different leak subtraction protocols affected the shape and amplitude of the peak, plateau, and tail currents, indicating that significant leak subtraction error is inherent in these astrocyte recordings (not shown). In some cases, a notch filter centered at 585 kHz was used. Access resistances (R_A) ranged from 20 to 50 MΩ; any cells with R_A beyond this range were excluded from analysis. Light pulses of 470-nm were delivered using a CoolLED Pe-2 (Andover, UK) and 470-nm LP excitation filters. Measurements of voltage-gated and neuronal-activity–induced astrocyte currents were averaged across two and four trials, respectively, within each cell. These responses were then averaged across cells and plotted using Prism software (GraphPad Software, La Jolla, CA). Looper-evoked motor neuron inhibitory postsynaptic current (IPSC) kinetics were analyzed in the Clampfit application of pClamp, rise and decay times were measured from 1/3 to 2/3 peak amplitude and from 2/3 to 1/3 peak amplitude, respectively, and fit was measured using a standard exponential with one term. Motor neurons were identified by referencing the morphological profiles of motor neurons with medially located cell bodies described in Choi et al. (2004).

Tissue preparation, immunolabeling, and imaging

Brains were fixed in 4% paraformaldehyde in 0.1 M PO_4 buffer, washed in PBS, and mounted in glycerol,

TABLE 1.
Summary of Experimental Genotypes

Figures	Genotype
1A	yw; P{w[+mC] = UAS-CD4-tdGFP}8M2; alrm-GAL4
1B–2E	w; P{w[+mC] = UAS-GFP.nls}14; alrm-GAL4
3A	yw; P{w[+mC] = UAS-CD4-tdGFP}8M2; D42-GAL4
3C,C1–3	w; P{w[+mC] = UAS-GFP.nls}14/+; D42-GAL4/+
3D–4C	w; UAS-ChR2-H134R; D42-GAL4
5A–C	w[1118]; P{y[+t7.7] w[+mC] = GMR50G08-lexA}attP40/+ ; P{y[+t7.7] w[+mC] = 13XLexAop2-IVS-myr::GFP}attP2 / +
5E,F; 6B	w[1118]; P{y[+t7.7] w[+mC] = GMR50G08-lexA}attP40, alrm-GAL4 / + ; P{y[+t7.7] w[+mC] = 13XLexAop2-IVS-Chrimson.mVenus}attP2 / +
6C	w[1118]; P{y[+t7.7] w[+mC] = GMR50G08-lexA}attP40, alrm-GAL4 / UAS-RNAiCG3747{attP,y[+],w[3′]}; P{y[+t7.7] w[+mC] = 13XLexAop2-IVS-Chrimson.mVenus}attP2 / +
6D, D1	w[1118]; +; alrm-GAL4/+
6D, D2	w[1118]; UAS-RNAiCG3747{attP,y[+],w[3′]} ; alrm-GAL4/+
8A; 8C	w[1118]; P{y[+t7.7] w[+mC] = GMR50G08-lexA}attP40, alrm-GAL4 / + ; P{y[+t7.7] w[+mC] = 13XLexAop2-IVS-Chrimson.mVenus}attP2 / +
8D	w[1118]; P{y[+t7.7] w[+mC] = GMR50G08-lexA}attP40, alrm-GAL4 / UAS-RNAiCG3747{attP,y[+],w[3′]}; P{y[+t7.7] w[+mC] = 13XLexAop2-IVS-Chrimson.mVenus}attP2 / +
8F	Black traces: same as in 8C. Teal traces: same as in 8D.

except for tissues with anti-dEaat1 immunolabeling, which were fixed in Bouin's fixative solution (Ramachandran and Budnik, 2010). Whole-mount preparations were mounted between two coverslips, using #1 coverslips as spacers to preserve tissue shape. For cross sections, brains were embedded in 8% low-melting-point agarose and cut at 80-μm thickness using a vibrating microtome. The following primary antibodies were used: anti-fasciclin II (FasII), anti-GFP, anti-*Drosophila* vesicular γ-aminobutyric acid (GABA) transporter (dvGat), anti-choline acetyl transferase (ChAT), anti-*Drosophila* vesicular glutamate transporter (dvGlut), and anti-dEaat1 (Table 2). For anti-FasII, anti-GFP, and anti-dEaat1 labeling, 2% bovine serum albumin (BSA) was used in a preincubation blocking step as well as during primary antibody incubation. For anti-dvGat and anti-ChAT labeling, 5% BSA was included in the blocking and primary incubation steps. No BSA was used for anti-dvGlut. Secondary antibodies included goat anti-mouse Cy-3 secondary antibody (Jackson ImmunoResearch, West Grove, PA) used at 1:200, and goat anti-rabbit Alexa Fluor 647 (Thermo Fisher Scientific) used at 1:400. Triton X-100 was included in all preincubation, primary, and secondary antibody steps to permeabilize tissue, at 0.2% for cross-sectioned and 0.5% for whole-mounted tissue. Syto 59 (1:20 K, 30 minutes; Thermo Fisher Scientific) was used to label cell nuclei. Confocal images were collected on a Zeiss (Thornwood, NY) 510 Laser Scanning Confocal Microscope and adjusted in Adobe Photoshop (San Jose, CA) using linear and/or gamma corrections.

Antibody characterization

Anti-FasII

The anti-FasII antibody labeled a 97-kDa band in western blot, which was absent in FasII null mutants (Grenningloh et al., 1991; Mathew et al., 2003). The labeling pattern observed in this study is identical to previous reports (Grenningloh et al., 1991; Landgraf et al., 2003; Mathew et al., 2003).

Anti-GFP

No labeling was observed in larval brains from flies lacking genetically encoded GFP expression (w^{1118}) (our observation, not shown).

Anti-dvGat

Western blots of head homogenates probed with an antibody to dvGat showed a single major band at 60 kDa. Cultured S2 cells expressing dvGat cDNA show punctate intracellular labeling with this antibody (Fei et al., 2010).

Anti-ChAT

The anti-ChAT antibody was shown to label a single band at a position of about 80 kDa in crude fly head samples (Takagawa and Salvaterra, 1996).

Anti-dvGlut

No labeling was observed in embryos homozygous for OK371ΔD, a chromosomal deficiency covering dvGlut (Mahr and Aberle, 2006).

Anti-Eaat1

Sera were tested by immunolabeling dissected central nervous system (CNS) tissues. The specificity of Eaat1 antiserum was confirmed by loss of Eaat1 immunoreactivity in Eaat1 null mutants (Peco et al., 2016).

TABLE 2.
Primary Antibodies Used in This Study

Antibody	Immunogen	Source, catalog no., species, type	Dilution	Reference, RRID
Anti-FasII	*Drosophila* fasciclin II	DSHB, Cat# 1D4 concentrate, mouse, monoclonal, MIgG1	1:400	Grenningloh et al., 1991 AB_528235
Anti-GFP	Green fluorescent protein	Molecular Probes, Cat# A21311, rabbit, polyclonal, Alexa Fluor 488-conjugated	1:450	AB_221477
Anti-dvGat	*Drosophila* vesicular GABA transporter C-terminal peptide (-CDSGNALINAFEIGLPF)	David Krantz, David Geffen School of Medicine at UCLA	1:400	Fei et al., 2010 AB_2313643
Anti-ChAT	*Drosophila* choline acetyl transferase	DSHB, Cat# chat4b1 supernatant, mouse, monoclonal	1:10	Takagawa and Salvaterra, 1996. AB_528122
Anti-dvGlut	*Drosophila* vesicular glutamate transporter N-terminal fragment (amino acids 2–87)	Hermann Aberle, Heinrich-Heine-Universität Düsseldorf, rabbit, polyclonal	1:200	Mahr and Aberle, 2006 AB_2490070
Anti-dEaat1	*Drosophila* excitatory amino acid transporter 1 (amino acids 117–195)	Donald van Meyel, McGill University Centre for Research in Neuroscience, rabbit, polyclonal	1:5K	Peco et al., 2016

Three-dimensional reconstruction from electron microscopy dataset

The third-instar larval VNC EM dataset was generated according to the methods outlined in Ohyama et al. (2015). Images were aligned using TrakEM software and annotated in the CATMAID user environment (Saalfeld et al., 2009) in which the looper population member A02m_a3l Pseudolooper-3 (located in segment A3, left) was completely skeletonized according to criteria in Ohyama et al. (2015), including full annotation of pre- and post-synaptic connections. Synapse-rich regions were identified, and image subsets that included all 67 presynaptic sites on the neuron were exported into *Reconstruct* (Fiala, 2005) for volumetric reconstruction. The profile of the looper neurite, all looper presynaptic sites, and the astrocytic processes surrounding the neurite were traced in each z section. An x–y area of at least 5 μm × 5 μm was reconstructed. These objects were exported to Amira v. 5.6 (http://www.amiravis.com; RRID: SCR_007353), where measurements from each point on the surface of the presynaptic site to the nearest astrocytic process were calculated. These distances were displayed visually using a colorimetric heat map, where red represents a distance of 0 μm; yellow, 0.5 μm; and blue, 1 μm. The smallest distance value for each presynaptic site is represented in the summary histogram.

Locomotion assays

Animals were reared and tested in conditions as described above, but in an environmental chamber with 50–70% humidity. Locomotion assays were performed on grape-juice agar (3%) plates by an individual who had been blinded to genotype. Female late third-instar larvae were collected from vials, transferred to plates, and then allowed to acclimate for at least 30 seconds before testing. Larvae were placed under a dissecting microscope to enable observation and counting of peristaltic contractions. A digital handheld counter and timer were used to record the number of contractions per minute. For each animal, three sequential 1-minute trials were conducted, and the results of each were averaged to yield a mean contraction rate.

Statistical analysis

Statistical analysis and graphing were carried out in GraphPad Prism unless otherwise noted. Astrocyte dye-coupling frequency in stimulated and unstimulated preparations was compared using Fisher's Exact Text. Recording duration distribution for coupled and uncoupled results were compared using an independent sample Kolmogorov–Smirnov test. The relationship between astrocyte holding potential and D42 neuron-evoked responses was examined using a bivariate correlation. Looper-evoked motor neuron IPSC parameters recorded in standard saline versus TBOA were compared using a paired two-tailed *t*-test. Looper-evoked motor neuron IPSC parameters recorded in control (alrm-GAL4) and *Eaat1*-knockdown conditions were compared using an unpaired two-tailed *t*-test. Locomotion-assay data were analyzed using a one-way analysis of variance (ANOVA) test.

RESULTS

Identification and intrinsic properties of third-instar larval astrocytes *in vivo*

The larval central nervous system consists of two brain lobes and the VNC. Each VNC segment corresponds with a segment of the larval body wall and is divided into two symmetrical hemisegments. The

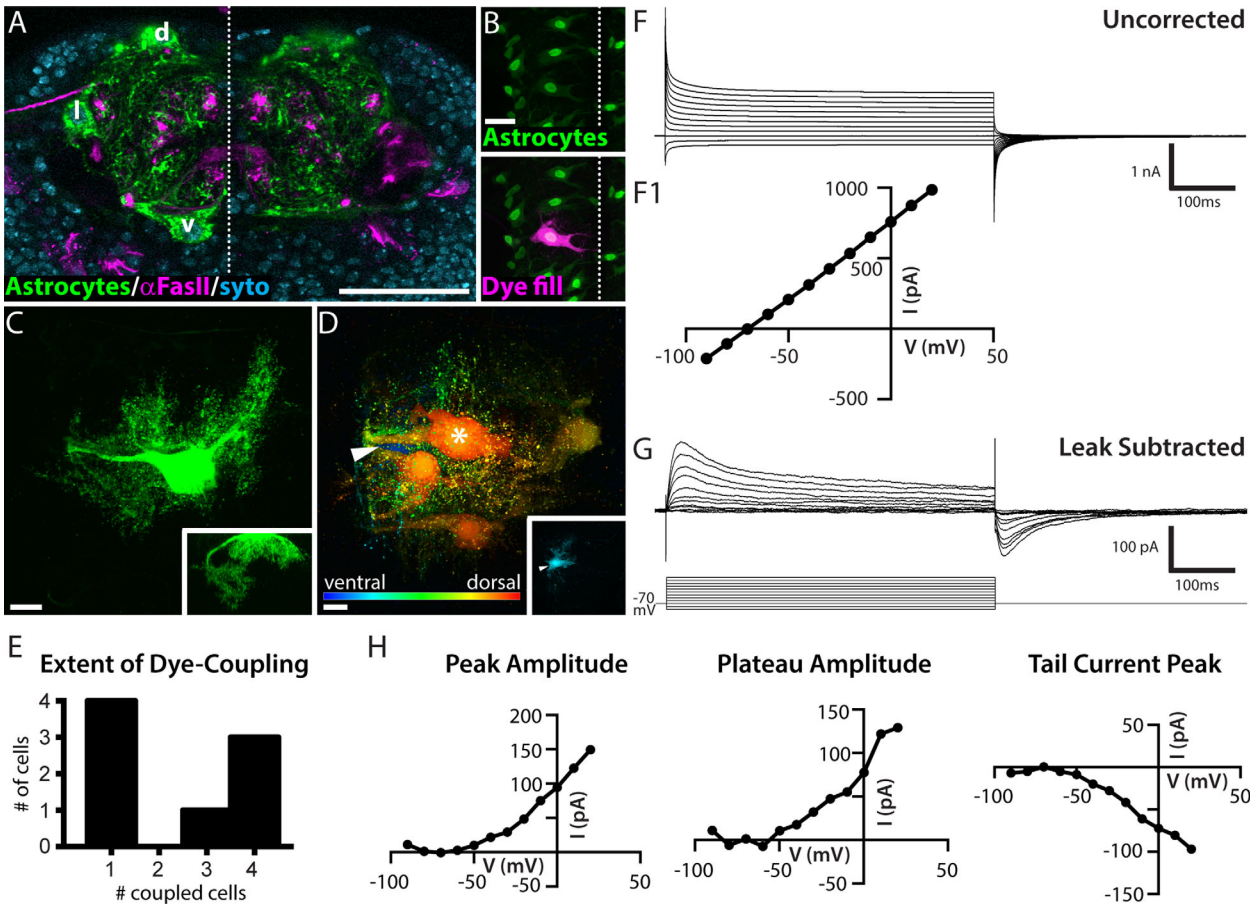

Figure 1. *Drosophila* astrocytes exhibit dye-coupling and passive membrane properties. **A:** Cross-sectional view of larval ventral nerve cord (VNC), 3rd thoracic segment, showing astrocyte membrane (green, alrm-GAL4>CD4-GFP), Fasciclin II–positive axon tracts (magenta), and cell nuclei (blue, Syto dye). Total substack thickness = 2.5 μm, astrocyte cell bodies located d, dorsally; l, laterally; v, ventrally; dotted line, midline. **B:** Dorsal view of whole-mount preparation showing astrocyte nuclei (green, alrm-GAL4>GFP.nls) and a dye-filled astrocyte (magenta). Dotted line, midline. **C:** Maximal projection of a dye-fill resulting in a single labeled astrocyte, dorsal view. Inset, cross-sectional view. **D:** Depth-coded image (red, dorsal; blue, ventral) of a maximal projection of a dye-fill showing four astrocytes in addition to the primary astrocyte from which the recording was made (asterisk). Arrowhead, blue cell body located ventrally. Inset, substack showing the same ventral cell body; overlying dorsal optical sections are omitted. Eight of the 26 cells examined displayed coupling. **E:** Histogram showing the extent of dye-coupling observed in eight cases in which coupling was present. **F:** Uncorrected whole-cell currents (mean, n = 8) recorded from a holding potential of −70 mV. **F1:** The corresponding current-voltage (I-V) plot indicates a linear I-V relationship (current measured 490 ms into the 500-ms pulse). **G:** Whole-cell currents (mean, n = 20) recorded as in E with leak current subtracted (online, P/4, opposite polarity). **H:** I-V plots for mean leak-subtracted trace shown in F. Current amplitude was measured at the peak of the outward current, at the plateau (10 ms before termination of the pulse), and at the peak of the tail current. Scale bar = 50 μm in A; 20 μm in B; 10 μm in C,D.

architecture of the VNC follows the general plan of the insect CNS (Fig. 1A). It is organized into two distinct compartments: the cortex, which contains all neuronal and glial cell bodies (nuclei in blue), and the neuropil, which contains neuronal processes, synapses, and astrocytic processes (green). Fasciclin II-positive axon tracts (magenta) are shown to provide landmarks within the larval VNC neuropil (Landgraf et al., 2003). *Drosophila* astrocytes were labeled by using the astrocyte-specific driver, alrm-GAL4, to express membrane-targeted GFP (Doherty et al., 2009). In the cross-sectional view of the third thoracic segment in Figure 1A, the cell bodies of 3 of the 12 astrocytes residing in that segment are visible; dorsal (d), lateral (l), and ventral (v) astrocyte cell bodies appear in the left hemisegment. Typically, an entire thoracic hemisegment includes three additional dorsal astrocytes but no additional lateral or ventral cells (our observation). These numbers are in close agreement with those of Stork et al. (2014) and Peco et al. (2016), in which a dorsomedial group (three cells), a dorsolateral group (two cells), and a single ventrally-positioned cell were described.

Drosophila astrocytes were targeted for recording by labeling cells with nuclear GFP expressed under the control of alrm-GAL4. Inclusion of dye in the recording electrode allowed us to confirm the identity of the recorded cell after each experiment (Fig. 1B). In the majority of cases (70% of astrocytes, $n = 26$), only the primary, recorded cell was filled with dye (Fig. 1C). In the remaining 30% of cases, *Drosophila* astrocytes displayed dye-coupling to one to four additional astrocytes within the hemisegment (Fig. 1D,E). The cell bodies of the dye-coupled astrocytes could be dorsal, lateral, or ventral in the hemisegment (Fig. 1D, inset). Dye-coupling was never observed to extend to astrocytes with cell bodies located in anterior, posterior, or contralateral hemisegments, nor was any dye-coupling observed between astrocytes and other types of glial cells, such as ensheathing and cortex glia. This suggests that the functional organization of the astrocyte network corresponds with the segmentally repeated neuronal circuitry, or "anatomo-functional compartments," of the larval VNC.

We hypothesized that the subset of astrocytes that were filled with dye during experiments in which neuronal activity was artificially increased (via channelrhodopsin expression under the control of the D42-GAL4 driver; see the section "Astrocyte response to broad neuronal network activity" below) would display a higher frequency of astrocyte dye-coupling (Roux et al., 2011). However, there was no difference between our sample of unstimulated preparations, in which 4 of 14 astrocytes were dye-coupled, and stimulated preparations, in which 4 of 12 astrocytes were dye-coupled. This result does not eliminate the possibility that activity from a certain neuronal cell type, or patterned in a certain manner, may dynamically regulate astrocyte coupling. In any case, our results are the first to demonstrate dye-coupling between *Drosophila* astrocytes, a hallmark feature of vertebrate astrocytes.

The mean membrane resistance (R_m) of a *Drosophila* astrocyte was 48.1 MΩ $\pm$ 27.8 SD, a value significantly lower than that of neighboring motor neurons, whose resistance was in the 1–1.5 GΩ range, as also reported by Choi et al. (2004). Measurements collected immediately after breaking into the cell show that *Drosophila* astrocyte membranes rest at a potential of ~ -70 mV. This potential is more hyperpolarized than that recorded in larval motor neurons (-55 to -60 mV, our observations, and Choi et al., 2004). The mean membrane capacitance (C_m) of individual (not dye-coupled) *Drosophila* astrocytes was 138.5 pF $\pm$ 44.9, and at -70 mV, the time constant (tau) for a 10-mV depolarizing pulse was 2.57 ms $\pm$ 1.16. This membrane capacitance value is approximately three times greater than what we have observed for motor neurons in this system. These parameters indicate that astrocytes possess a large, but leaky, surface area. Their morphology reinforces this notion; each astrocyte has three to four thick primary processes, some of which travel along the cortex–neuropil boundary for some distance before entering the neuropil. Once in the neuropil, astrocytic processes exhibit a tufted morphology with finely branched, often veil-like, distal processes (Fig. 1C). Given these morphological and electrical properties, we assume that our cell-body recordings are unlikely to detect activity in the distal-most branches.

Drosophila astrocytes lack detectable voltage-gated currents

Astrocytes were voltage-clamped at -70 mV and stepped from -90 mV to $+20$ mV for 500 ms in 10-mV increments. The resulting current-voltage (I-V) relationship is roughly linear and indicative of a large leak current (Fig. 1F). Subtraction of the leak current eliminated the linear current response between -90 and -60 mV and revealed a small net-outward current with two apparent temporal components in response to depolarizing pulses (Fig. 1G): a fast, transient current that reaches its peak amplitude 16–20 ms after depolarization, and a sustained component. Upon returning to -70 mV, an inward tail current is activated. These leak-subtracted currents are 10-fold smaller than the uncorrected amplitudes, and retain an approximately linear I-V relationship between -50 mV and $+20$ mV (Fig. 1H).

We investigated the ionic bases of the fast peak and the plateau using 100-ms voltage steps and a battery of ion-substitution protocols and well-characterized pharmacological agents that block voltage-gated sodium and potassium channels. The recordings showed modest variation in the absolute and relative amplitude of each component across individual cells "before" drug, and subtle, but inconsistent changes in the amplitude and kinetics of the fast transient, sustained outward, and fast inward tail current in response to the particular saline solution or agent applied (Fig. 2A–E). No systematic effect of any drug was observed across cells. These observations led us to propose that the signal remaining after leak subtraction does not contain any significant voltage-gated current; instead, the membrane properties of astrocytes, which allow 10- to 20-fold more current leakage than do neurons in this system, perhaps generate an axial-current flow between non-isopotential cell compartments (ΔVm at the soma and proximal processes $>$ ΔVm at distal processes, creating a potential difference that drives negative current toward the electrode) in the voltage-clamp configuration that is not accurately subtracted by our methods. The transient, larger amplitude current observed in leak-

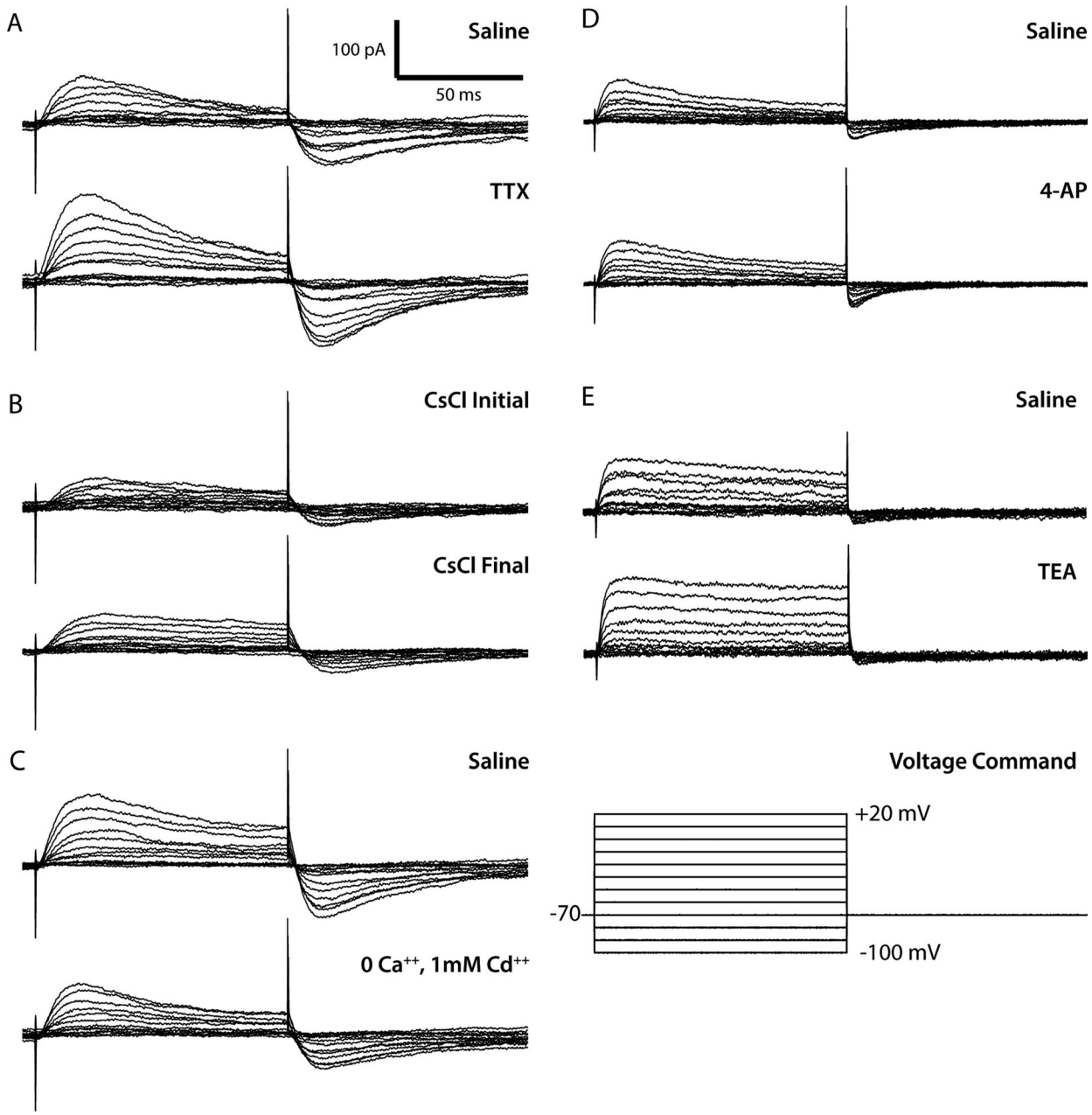

Figure 2. Voltage-gated currents were not detected in larval VNC astrocytes. All data shown in this figure are representative traces from one of a group of three to five astrocytes in each set. Traces were generated using online P/4 opposite-polarity leak subtraction. **A:** Top: whole-cell voltage-clamp current recorded from a single cell in standard solution. Bottom: current recorded during subsequent perfusion with TTX. **B:** Top: current recorded immediately after breaking into the cell with a CsCl pipette solution. Bottom: current recorded from the same cell 10 minutes after cell break-in. **C:** Top: current recorded in standard solution. Bottom: current recorded during subsequent perfusion with 0 Ca^{2+}, 1 mM Cd^{2+}. **D:** Top: current recorded in standard solution. Bottom: current recorded during subsequent perfusion with 4-AP. **E:** Top: current recorded in standard solution. Bottom: current recorded during subsequent perfusion with TEA.

subtracted traces during the first 20 ms of a depolarizing step may thus represent the larger initial potential difference between the soma and distal processes, which eventually reaches equilibrium at around 40 ms. In summary, we did not find evidence of any significant voltage-gated current in third-instar larval VNC astrocytes.

Astrocyte response to broad neuronal network activity

We next asked whether *Drosophila* astrocytes respond to neuronal activity. Neurons were activated optogenetically using the D42-GAL4 neuronal driver, which was selected because it has high GAL4 expression levels and defines a restricted yet heterogeneous

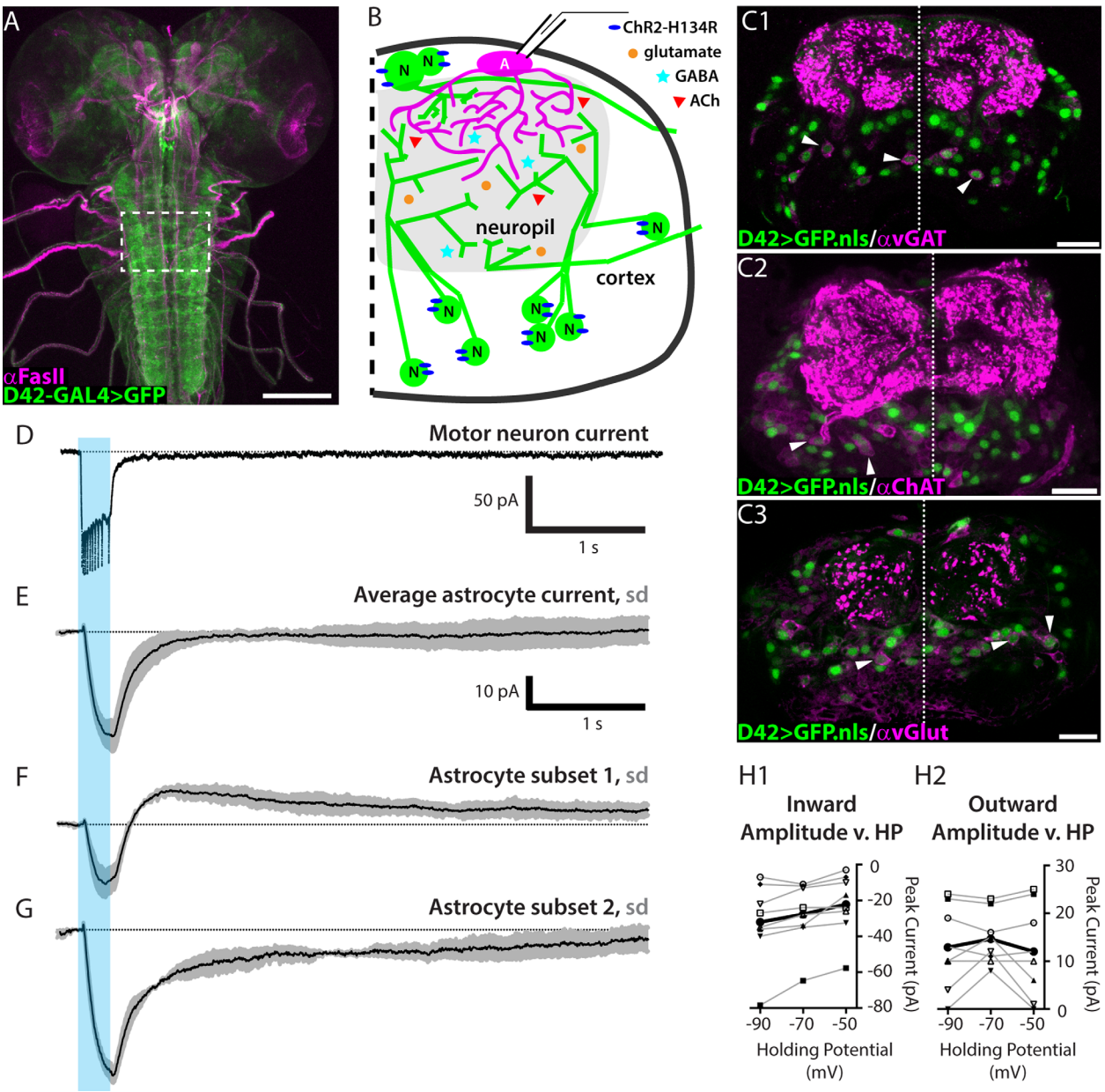

Figure 3. Neuronal activity induces an inward current as well as a current with slow kinetics and variable polarity. **A:** D42 neuronal driver expression pattern (green) and Fas II landmarks (magenta) in a whole-mount third-instar larval CNS. Recordings were made from cells within the segments enclosed by the dashed box. **B:** Schematic diagram for experiments: channelrhodopsin is expressed in a heterogeneous neuronal population (green) using the D42 driver; whole-cell recordings are collected from dorsal astrocytes (magenta). **C1–C3:** Cross-sectional view of D42-GAL4>nuclear GFP (green) and anti-vGAT (C1), anti-ChAT (C2), or anti-vGlut (C3) immunolabeling pattern (magenta). Arrowheads highlight selected D42 nuclei surrounded by transmitter-identifying immunolabeling. Dotted line, midline. Total substack thickness = 2.5 μm. **D.** Voltage-clamp recording from a channelrhodopsin-expressing motor neuron (representative trace, $n = 10$ preparations). Unclamped spikes are triggered by a 250-ms blue-light stimulus (470 nm, blue bar). Dotted line, baseline. **E:** Mean current from 31 astrocytes. Blue-light activation of neurons yields an inward glial current that follows by 25 ms. Gray, SD. **F,G:** Mean current from two subsets of cells sorted by response profile to optogenetic stimulation. **F:** In one subset, the current transiently overshoots baseline before returning over 4 s, $n = 18$. **G:** In the second subset, the current rises to baseline over 4 s, $n = 13$. **H1:** Shows a weak positive relationship between holding potential and peak amplitude of the fast inward current ($r = 0.219$). **H2:** No relationship between holding potential and the amplitude of the slow, variable-polarity current ($r = -0.046$). Black, mean of eight cells. Gray, individual cells. Scale bar = 100 μm in A; 20 μm in C1–C3.

population of larval VNC neurons (Fig. 3A–C). D42-GAL4–expressing neurons ("D42 neurons") are heterogeneous in transmitter type; immunolabeling for the vesicular GABA and glutamate transporters, as well as choline acetyl transferase, indicates that the D42 population comprises at least cholinergic, glutamatergic, and

GABAergic neurons (Fig. 3C). D42 neurons are also heterogeneous with respect to neuronal cell class, including many interneurons, a subset of sensory neurons, and some motor neurons. The motor neurons, which are glutamatergic, are not known to make any presynaptic connections within the CNS, and thus may not be relevant to local astrocyte responses to neuronal activity (Schneider-Mizell et al., 2016). Channelrhodopsin (ChR2-H134R; Pulver et al., 2009) was used to stimulate D42 neurons. To determine an optimal stimulus duration, we presented optical stimuli of different durations while recording from select D42-GAL4–expressing motor neurons with medially-located cell bodies (RP2 and aCC). Attenuation of neuronal firing rate was used to determine that 250 ms was an appropriate stimulus duration to elicit maximal firing with minimal adaptation of firing frequency (Fig. 3D). Note that in the D42-GAL4>ChR2-H134R experiments, two copies of the GAL4 driver and UAS construct were needed to obtain sufficient expression levels/depolarization to trigger motor neuron spikes.

In subsequent experiments, D42 neurons were again stimulated for 250 ms, but the patch electrode was targeted instead to astrocytes (Fig. 3B,E). Astrocytes were reliably identified by using the intrinsic properties (Rm, Cm, tau, non-spiking, linear voltage-activated currents) defined earlier and subsequently confirmed using Alexa Fluor dye fills. D42 neuronal activity elicited an inward current present for the duration of the light stimulus (Fig. 3E). The mean amplitude of this inward current was −37.7 pA ± 17.3. The onset of astrocyte depolarization was delayed significantly relative to neuronal activity, occurring 35 ms after ChR2-mediated neuronal depolarization began and 25 ms after the first spike was recorded from the medial motor neurons.

The astrocyte current shown in Figure 3E represents the mean of all 31 cells in this experimental series. For the group, the mean current returns to baseline 1.5 seconds after termination of the stimulus. However, the current of an *individual* cell rarely returned to baseline within 1.5 seconds. We classified the responses into categories that illustrate the two extremes; these profiles are shown separately in Figure 3F ($n = 18$) and G ($n = 13$). In one subset (Fig. 3F), the peak of the fast inward current slightly precedes the offset of light-induced neuronal activity and is followed by a net outward current that slowly returns to baseline, reaching it about 4 seconds after stimulus offset. In the second subset (Fig. 3G), the peak inward current coincides with the termination of the stimulus, and there is a net inward current that slowly returns to baseline over an identical time course of about 4 seconds. We note that a given cell's current profile could be dynamic during the session, namely, the polarity and amplitude of the slow current changed over time in 12 of 31 cells examined.

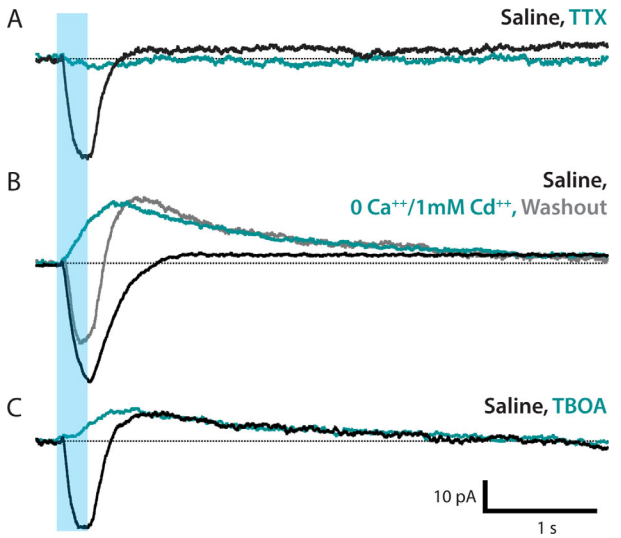

Figure 4. Neurotransmitter release evokes an inward glutamate transporter current. Representative traces, $n = 5–6$ cells in each group. **A:** TTX completely blocks the inward current associated with neuronal stimulation (teal). **B:** Neurotransmitter release blocked using a 0 Ca^{2+}, 1 mM Cd^{2+} bath (teal). Inward current is abolished and an outward current is induced/potentiated. Saline washout restores the inward current; outward current remains (gray). **C:** Inward current is completely blocked by glutamate transporter antagonist TBOA (teal); slow outward current is not affected.

Fast inward neuronal-activity–evoked astrocyte currents are mediated by glutamate transporters

Next, we asked whether the astrocyte response to neuronal activity is dependent on neurotransmitter release. Bath application of TTX during optical-stimulation experiments blocked all astrocyte current in all trials (Fig. 4A). This effect is mediated by blockade of Na_v channels in neurons, as we did not find evidence for Na_v in astrocytes (Fig. 2A). This blockade did not reverse upon washout with normal saline, consistent with observations in other insect nervous systems that TTX binds the neuronal voltage-gated sodium channel irreversibly (Hayashi and Levine, 1992). Blocking neurotransmitter release with a zero Ca^{2+} and 1 mM Cd^{2+}solution blocked the fast, inward current in all trials; the slow current either appeared with outward polarity or was preserved as an outward current. Upon washout with normal saline, the fast inward current returned; the slow outward current remained at the conclusion of a 10-minute washout (Fig. 4B).

Because there are glutamatergic synapses in the *Drosophila* VNC neuropil (Fig. 3C,C3 and Mahr and Aberle, 2006), we hypothesized that this fast inward current would be mediated by a glutamate transporter. Glutamate transporter currents derive from the co-transport of three Na^+, one H^+, and one glutamate (–) into the cell and one K^+ out of the cell and are thus net-inward (Shimamoto et al., 1998). We applied D,L-TBOA, a high-affinity competitive antagonist of excitatory amino acid transporters that does not affect ionotropic or metabotropic receptors (Shimamoto et al., 1998). We found that TBOA completely blocked the fast inward current in *Drosophila* astrocytes, supporting the conclusion that this current is mediated by glutamate transporters (Fig. 4C). Consistent with its dependence on ionic gradients, we found a weak positive relationship between the amplitude of the inward glutamate transporter current and holding potential ($r = 0.219$; Fig. 3H,H1).

Slow variable-polarity neuronal-activity–evoked astrocyte currents reflect potassium buffering

TBOA did not block the slow neuronal-activity–induced current (Fig. 4C), and we found no correlation between the amplitude of the outward slow current and holding potential ($r = -0.046$; Fig. 3H,H2); inward slow currents were excluded from this analysis due to the confounding effect of the fast inward current's offset kinetics. This insensitivity to holding potential suggests that this signal originates beyond the spatial extent of the voltage-clamped membrane. When the variable polarity of the slow current and its sensitivity to TTX, but not Cd^{2+} or TBOA, are taken together, these data indicate that the slow current depends on the Na^+/K^+ flux generated by neuronal activity. Our results are consistent with the hypothesis that the slow astrocyte current reflects a dynamic response to neuronal-activity–mediated changes in the concentration and distribution of extracellular potassium. Thus, we suggest that this current is indicative of potassium-buffering.

Looper-to-motor neuron connections are mediated by glutamate-gated chloride channels

To further examine the astrocytes' response to synaptically released glutamate, we performed a series of experiments in which we expressed a channelrhodopsin with improved properties, Chrimson (Klapoetke et al., 2014), in a population of glutamatergic interneurons. The neurons in this population are called "loopers" here, in reference to the looped morphology of their primary neurite (Fig. 5A,B). Loopers have ventromedially-located somas (14 cells per hemisegment), receive inputs in the sensory neuropil, and make outputs, as well as receive some additional inputs, in the dorsal motor neuropil (Fig. 5D). The wiring diagram derived from a first-instar 3D EM dataset confirms that loopers make direct synaptic connections with some medial motor neurons, including RP2 (also termed MNISN-Is) (Schneider-Mizell et al., 2016). Terminal looper neurites located in the motor neuropil were labeled by an antibody to the vesicular glutamate transporter protein dvGlut (Fig. 5C).

Our physiological data reaffirm that the looper-to-RP2 connection persists in the third instar (Fig. 5E). In addition to RP2, we also detected looper-evoked IPSCs in whole-cell recordings from RP3 (MN6/7-Is) (Fig. 5F,G). Note that glutamate signaling in the fly CNS differs from that of vertebrates due to the presence of inhibitory glutamate receptors. Previous studies have shown that motor neurons express glutamate-gated chloride channels (Rohrbough and Broadie, 2002), which have been characterized in other invertebrates such as *Caenorhabditis elegans* (Vassilatis et al., 1997) but are absent from vertebrate genomes (Wolstenholme, 2012). The *Drosophila* homolog of this receptor, *GluCl-alpha*, produces a glutamate-gated chloride current when cloned and expressed in *Xenopus* oocytes (Cully et al., 1996).

In agreement with each of these findings, and other studies concluding that glutamate's action in the *Drosophila* CNS is inhibitory (Liu and Wilson, 2013; Kohsaka et al., 2014), looper-evoked motor neuron IPSCs are blocked by picrotoxin and have a reversal potential of –80 mV (Fig. 5E–G). When taken together with this literature, our immunolabeling, electrophysiology, and pharmacology results show that synaptic communication between looper neurons and motor neurons is mediated by glutamate-gated chloride channels.

Astrocyte glutamate transport is mediated by Eaat1

One would expect looper activation, which releases glutamate in the dorsal neuropil, to activate a glutamate transporter current in nearby astrocytes. To test this, whole-cell patch-clamp recordings were collected from astrocytes while looper neurons were activated (Fig. 6A). This elicited an inward current with a mean amplitude of -15.57 pA, $\pm$ 3.75 that was completely blocked by bath application of TBOA (Fig. 6B). The mean amplitude is smaller and shows less variation than the mean inward amplitude for D42 neuronal activation, as would be expected with activation of a smaller group of glutamatergic neurons. The slow

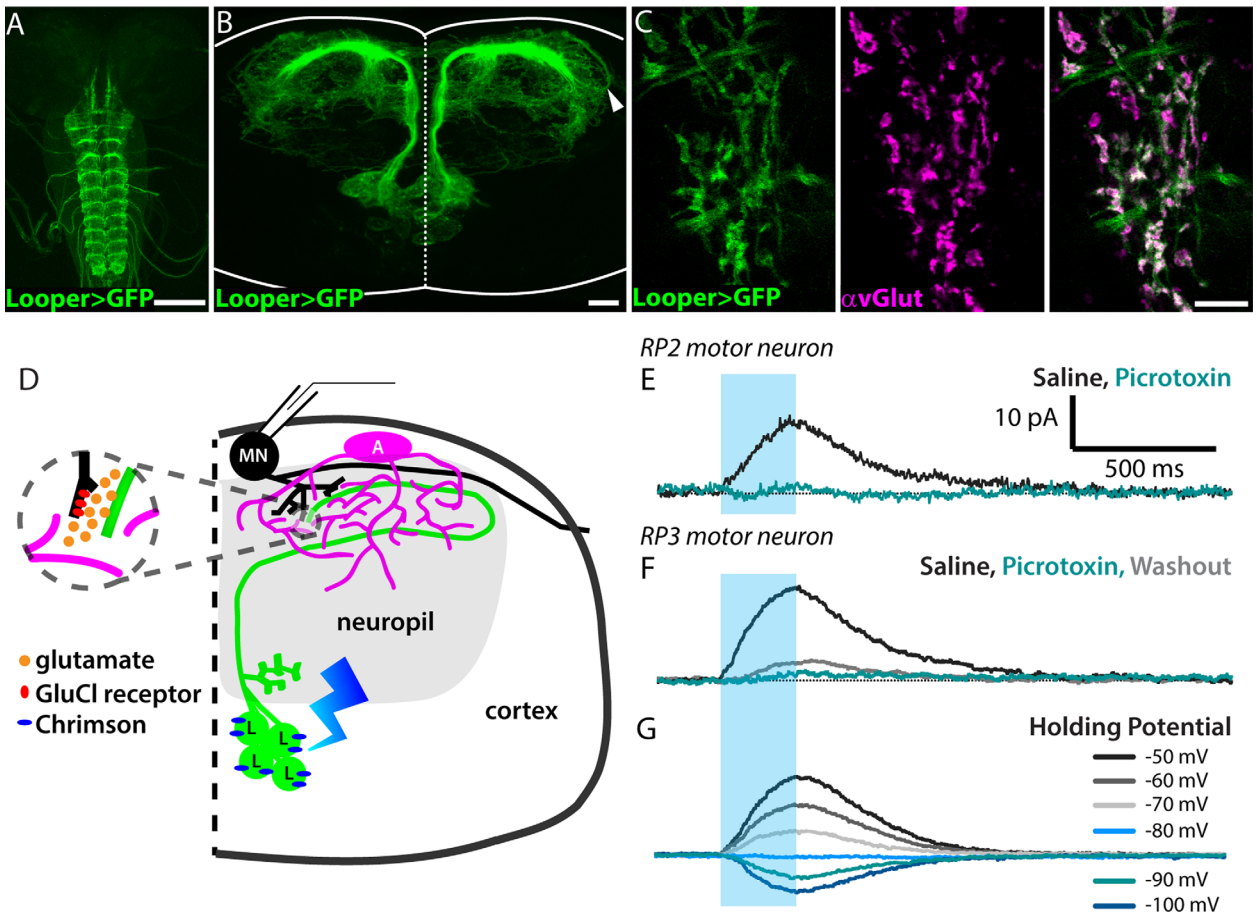

Figure 5. Looper–motor neuron synaptic communication is mediated by a glutamate-gated chloride-channel receptor. **A:** Whole-mount third-instar larval CNS showing the VNC expression pattern of the Looper driver (green, Looper-LexA>membrane GFP). **B:** Cross-sectional view of the looper neurons (green); dotted line, midline; solid line, tissue boundary. Substack encompasses cells in thoracic segment 2, total thickness = 73 μm. Arrowhead, looped tract shown in schematic diagram in E. **C.** Dorsal view of a single optical section (z = 0.5 μm) showing colocalization of looper membrane (green) and dvGlut antibody labeling (magenta). Green-only regions in merged image are looper tracts, where no synapses are expected. **D:** Schematic diagram illustrating the presynaptic glutamatergic neuron (Looper, "L", green) expressing Chrimson (blue), an adjacent astrocyte ("A", magenta), and a postsynaptic motor neuron ("MN", black) from which recordings shown in E–G were collected. **E:** Optical stimulation of looper neurons (blue bar, stimulus window) during a whole-cell voltage-clamp recording (holding potential = −60 mV) from motor neuron RP2 reveals an IPSC in standard saline (black) that is blocked by bath-applied picrotoxin (teal). No washout was observed after 10 minutes. **F:** As in E, but recorded from motor neuron RP3. Some current returns upon washout (gray). **G:** Looper-evoked RP3 motor neuron IPSCs reverse at a holding potential of −80 mV. Scale bar = 100 μm in A; 10 μm in B,C.

current with variable polarity (potassium-buffering current) observed in response to activation of D42 neurons was not observed in response to looper activation. This is consistent with the idea that looper activation recruits far fewer neurons, which would elevate $[K_o]$ to a lesser degree.

In these experiments, we expressed Chrimson in looper neurons using the LexA system, while the GAL4/UAS binary system was used to manipulate the glutamate transporter *Eaat1* specifically in astrocytes with alrm-GAL4. In the presence of looper-LexA>Chrimson, the knockdown of astrocyte *Eaat1* completely eliminated the inward current observed in response to looper activation in controls (Fig. 6C). To confirm the specificity and efficacy of the RNAi hairpin, we performed Eaat1 immunolabeling in both control and alrm-GAL4>*Eaat1*^{RNAi} larval brains. Eaat1 labeling was robust in controls and almost completely eliminated in alrm-GAL4>*Eaat1*^{RNAi} samples (Fig. 6D). Taken together, these experiments identify glutamate transporters as a highly conserved mediator of neuron–astrocyte interaction.

The known lethality of null mutations in *Eaat1* (Stacey et al., 2010) and the pronounced phenotypes in flies with pan-glial-cell RNAi-knockdown of *Eaat1* (repo-GAL4) (Rival et al., 2004, 2006) led us to test alrm-GAL4>*Eaat1* ^{RNAi} larvae for gross locomotor defects. We did not detect any changes in contraction rate (mean ± SD contractions per minute = 40.2 ± 20.0

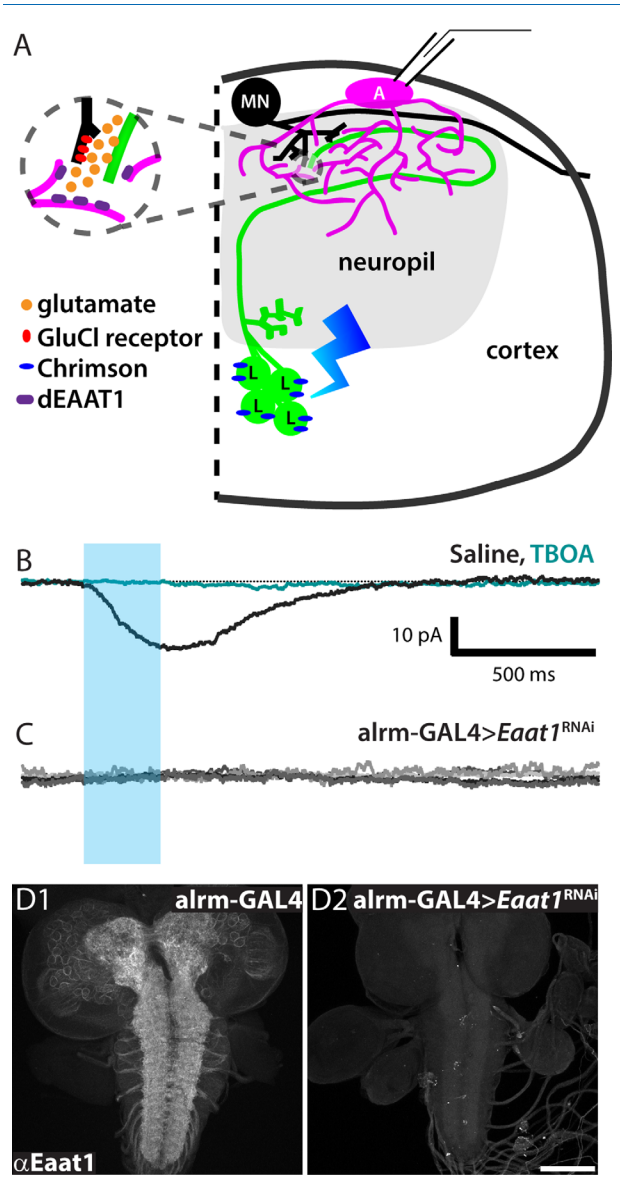

Figure 6. Astrocytes respond to glutamatergic neuronal activity with an Eaat1-mediated transporter current. **A:** Schematic diagram illustrating the presynaptic glutamatergic neuron (Looper, "L", green) expressing Chrimson (blue), the postsynaptic motor neuron ("MN", black), and an adjacent astrocyte ("A", magenta), from which recordings shown in B and C were collected. **B:** Representative whole-cell astrocyte recording in control genotype (Looper-LexA>Chrimson, alrm-GAL4). Black, standard saline perfusion. Teal, during perfusion with TBOA. Blue bar, optical-stimulus window. n = 5. **C:** Whole-cell astrocyte recordings collected from experimental genotype (Looper-LexA>Chrimson, alrm-GAL4>*Eaat1*^{RNAi}). Five overlaid traces show no response to looper activation. **D:** Whole-mount third-instar larval CNS labeled with rabbit-anti-Eaat1. **D1:** alrm-GAL4 control shows labeling throughout neuropil regions. **D2:** alrm-GAL4>*Eaat1*^{RNAi} shows little to no Eaat1 labeling. Scale bar = 100 μm in D2 (also applies to D1).

for UAS-*Eaat1*^{RNAi} controls, 46.6 ± 10.5 for alrm-GAL4 controls, and 41.2 ± 13.1 for alrm-GAL4>*Eaat1*^{RNAi}; n = 7 in each group, n.s.). Locomotor behavior, measured as contractions per minute, is thus grossly normal in alrm-GAL4>*Eaat1*^{RNAi} larvae.

Drosophila astrocytic processes are found within 1 μm of looper synapses but do not ensheathe them

After observing astrocyte responses to looper neurons' synaptically released glutamate, we wanted to investigate the anatomical relationship between *Drosophila* astrocytic processes and looper synapses in this neuropil. We identified one member of the same population of neurons (loopers) used in the electrophysiology experiments described above in a 3D EM dataset that spans third-instar larval VNC segments A2–A4. To link the specific anatomy of looper synapses and astrocytic processes to our experimental physiology results, we first identified all 67 presynaptic sites on this particular looper neuron. Then we volumetrically reconstructed the looper neurite, all of its presynaptic sites, and the surrounding astrocytic processes. The resultant 3D model (Fig. 7A) illustrates the dense feltwork of astrocytic processes present within the third-instar larval VNC neuropil. This model was used to measure the distance from each point on the extracellular surface of the presynaptic site to the nearest astrocytic process. The shortest-distance value for each presynaptic site ranged from 0.0006 to 0.93 μm, with a mean of 0.375 μm ± 0.2 (Fig. 7B). These distances were used to generate a heat map that illustrates the range across presynaptic sites as well as within a given presynaptic site (Fig. 7C–E). Complete ensheathment of a looper presynaptic site was never observed; in 2 cases (out of 67) the astrocytic process was close enough to the presynaptic site to be considered in direct contact. Our physiology results demonstrating astrocyte glutamate transporter currents in response to looper activation thus suggest that distances of up to at least 1 μm allow for communication between neurons and astrocytes.

Loss of astrocyte glutamate transport extends looper-evoked motor neuron IPSCs

Given these anatomical parameters, we next asked what effect blocking astrocyte glutamate transporters, either pharmacologically or genetically, has on looper-to-motor neuron communication. To address this question, looper-evoked motor neuron IPSCs were recorded in standard saline, and then exposed to TBOA, the same drug that blocked looper-evoked glutamate transporter currents in the astrocytes. This acute glutamate transporter block slowed the decay of IPSCs (Fig. 8A), significantly increasing IPSC half-width time, decay time, and the time constant resulting from a single

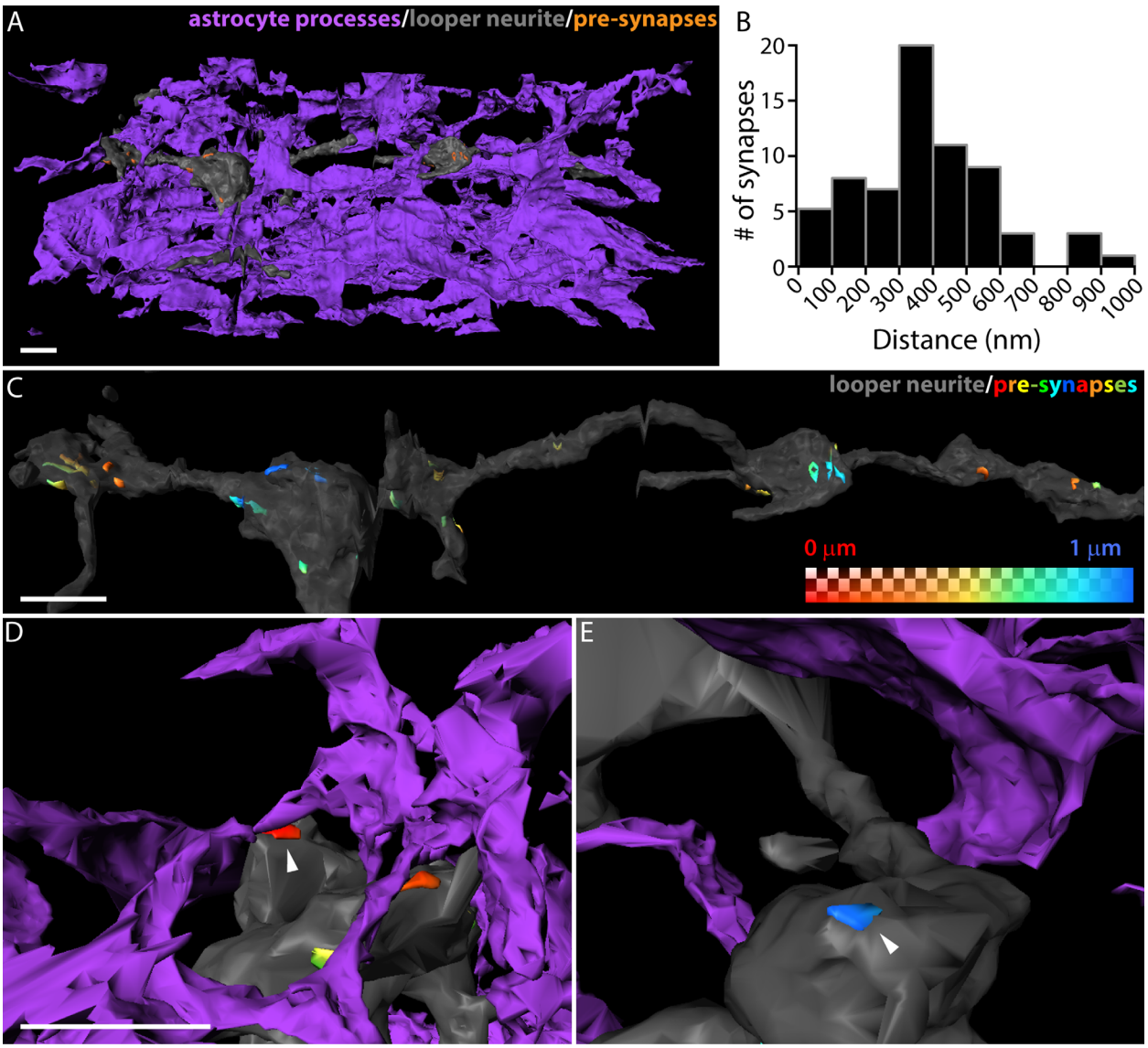

Figure 7. Astrocytic processes are found within 1 μm of looper presynaptic sites but do not ensheathe them. **A:** Three-dimensional reconstruction of a portion of the looper neurite (gray), and the surrounding astrocytic processes (purple). Some of the looper presynaptic sites are visible (orange). **B:** Distribution of shortest distance from a given active zone to nearest astrocytic process. All presynaptic sites on a fully reconstructed cell are included (mean = 375 nm ± 200 nm, n = 67). **C–E:** Reconstructed looper neurite; presynaptic sites are labeled with a heat map indicating the distance to the nearest astrocytic process. **C:** Astrocyte-process-to-presynaptic-site distance does not vary uniformly with location of the synapse on the neurite. **D:** Synapse at the minimum distance in the distribution (0.0006 μm, arrowhead) makes glancing contact with the presynaptic site. The astrocytic process does not ensheathe the synapse. **E:** Synapse from another neurite at the maximum distance in the distribution (0.93 μm, arrowhead). Scale bar = 1 μm in A, C, D (also applies to E).

exponential fit (Fig. 8B); no changes were found in IPSC rise time or amplitude (not shown).

A similar, but less dramatic, extension of the decay kinetics was observed when looper-evoked motor neuron IPSCs from control brains (normal Eaat1 levels) were compared with those from experimental brains with reduced Eaat1 levels (alrm-GAL4>*Eaat1*^{RNAi}) (Fig. 8C,D). Although the degree of change was attenuated in this chronic *Eaat1* knockdown condition compared with the acute, pharmacological block, changes in the IPSC half-width time, decay time, and the time constant of a single exponential fit remained significant (Fig. 8E), and again, rise time and amplitude were unchanged (not shown). Among the 10 motor neuron recordings shown for the control and 8 motor neuron recordings shown for the experimental genotype in Figure 5C and D, respectively, the resultant dye-fills confirmed that three of the recordings in each group were from the motor neuron RP2 (MNISN-Is). Four of the remaining motor neurons in each group were identified as RP3/

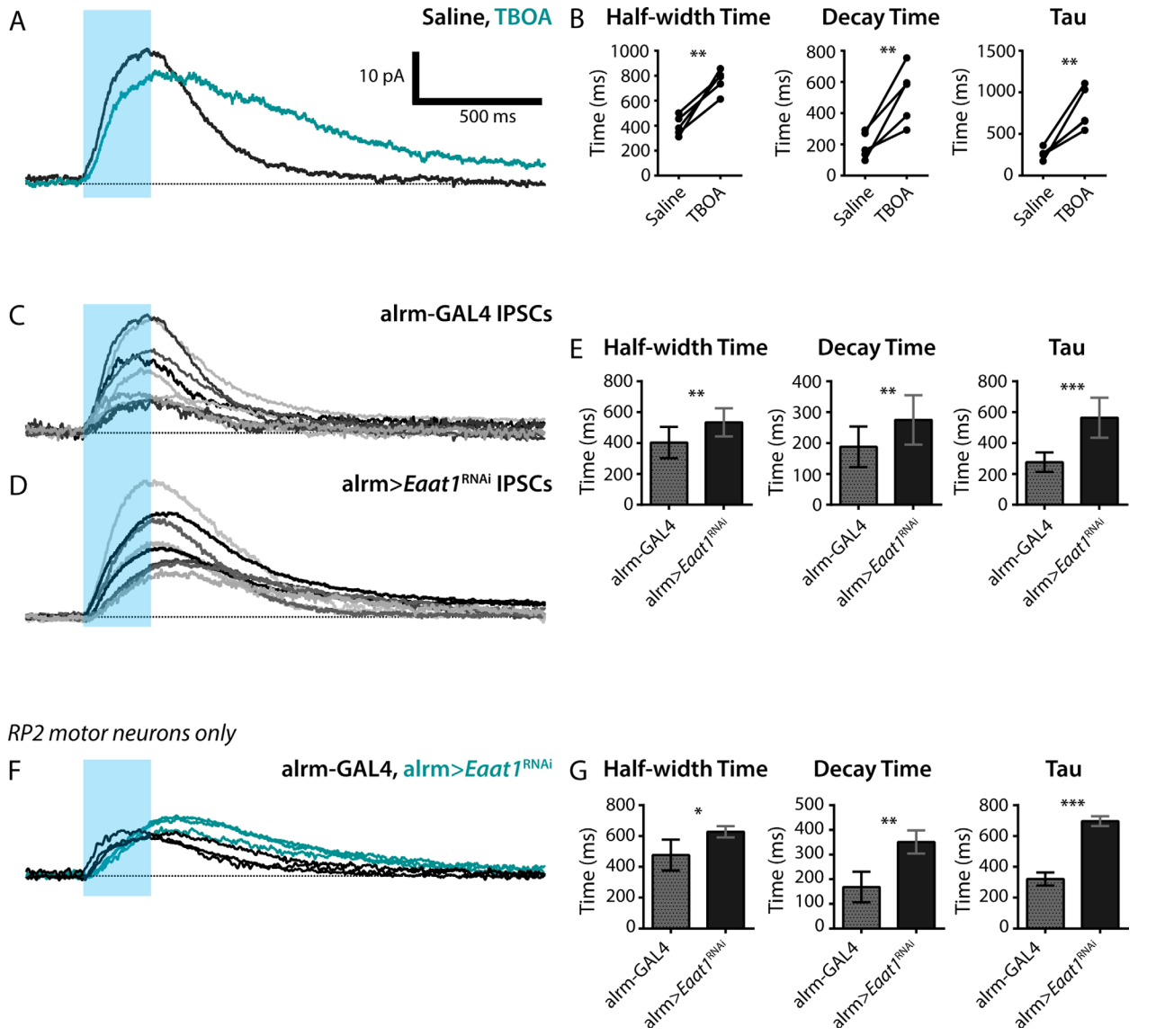

Figure 8. Astrocyte-specific Eaat1 knockdown significantly prolongs IPSCs at the looper-MN synapse. **A:** Optical stimulation of looper neurons (blue bar, stimulus window) during a whole-cell voltage-clamp recording results in motor neuron IPSCs. Standard saline (black), bath-application of the glutamate-transporter blocker TBOA, (teal). Representative trace from one of five preparations. **B:** IPSC half-width time, decay time, and time constant (fit with a single exponential function) are shown for five data pairs in control and TBOA conditions. **, $P < 0.01$; ***, $P < 0.001$. **C:** Looper-evoked motor neuron IPSCs from 10 control larval VNCs. **D:** Looper-evoked motor neuron IPSCs from eight larval VNCs with reduced astrocyte Eaat1. *Note:* both control and experimental genotypes also include Looper-LexA>Chrimson. **E:** Mean half-width time, decay time, and time constant for control and alrm-GAL4>*Eaat1*^{RNAi}. Error bars, ± SD. **, $P < 0.01$; ***, $P < 0.001$. **F,G:** A subset of the data shown in C and D demonstrates that the kinetic parameters in E remain significant when only recordings from motor neuron RP2 are considered. **F:** Recordings from control (black, $n = 3$) and alrm-GAL4>*Eaat1*^{RNAi} (teal, $n = 3$) are overlaid to facilitate direct comparison of IPSC kinetics. Blue bar, light stimulus. **G:** Analysis of kinetics of looper-evoked motor neuron IPSCs. Mean ± SD. *, $P < 0.05$; **, $P < 0.01$; ***, $P < 0.001$.

MN6/7-Ib, one was MNSNb/d-Is, and the remaining three were unidentifiable post experiment due to incomplete dye-fills. This subset of RP2-only recordings was analyzed independently and replicated the results of the larger dataset containing motor neurons of heterogeneous identity (Fig. 8F,G), except for the addition of a significant increase in IPSC amplitude in alrm-GAL4>*Eaat1*^{RNAi} preparations ($P < 0.05$, not shown).

DISCUSSION

The subset of *Drosophila* glial cells examined in this study has been named *interface glia* (Ito et al., 1995),

longitudinal glia (Beckervordersandforth et al., 2008), *astrocyte-like glia* (Awasaki et al., 2008), and, most recently, just *astrocytes* (Stork et al., 2014; Muthukumar et al., 2014; Peco et al., 2016), based on their morphology and molecular identity. The present study is the first to characterize the electrical membrane properties of *Drosophila* astrocytes. These whole-cell recordings indicate strong conservation of basic astrocyte properties across fly and vertebrate nervous systems, thus strengthening the argument that *Drosophila* astrocytes can be used to address very targeted and complex questions about general neuron–glia interactions. With these similarities in mind, our pairing of neuronal optogenetics and astrocyte electrophysiology with 3D EM provides insight into critical anatomical determinants of neuron–glia interactions.

Drosophila astrocyte intrinsic properties are similar to those of vertebrate astrocytes

The linear I-V relationship, indicating passive membrane conductance as first noted by Kuffler and Nicholls (1966), has emerged as a common property of astrocytes across species (*humans:* Schroder et al., 2000; Han et al., 2013; *rat:* Steinhauser et al., 1994; Kressin et al., 1995; Bergles and Jahr, 1997; Clark and Barbour, 1997; Zhou and Kimelberg, 2000, 2001; Zhang et al., 2009; Uwechue et al., 2012; Huda et al., 2013; *mouse:* Matthias et al., 2003; Lalo et al., 2006; *caiman:* Zayas-Santiago et al., 2014). Much like the astrocyte membranes in each of these species, the fly astrocyte has a resting membrane potential that is similar to or more negative than the potassium equilibrium potential, low membrane resistance, and high membrane capacitance. While there has been some debate as to whether the passive-membrane property of astrocytes is truly cell-intrinsic, or rather derives from an extensively-coupled astrocyte network, we note in our recordings from *Drosophila* astrocytes that the large leak currents found in uncoupled cells were comparable to those recorded from cells later found to be dye-coupled to other astrocytes. This result is in agreement with a careful study of rat astrocytes conducted by Schools et al. (2006), and we similarly conclude that these passive properties are cell-intrinsic and do not derive from the coupled network.

While astrocytes studied *in vitro* or in immature brain tissues display voltage-gated currents, those in mature, *in vivo* tissues overwhelmingly do not (Kafitz et al., 2008; reviewed in Ransom and Giaume, 2013). Here, we find little evidence for a significant voltage-gated current in third-instar *Drosophila* VNC astrocytes. The voltage-activated current remaining after leak subtraction is insensitive to Ca^{2+} and K^{+} ion substitution and pharmacological agents that block voltage-gated sodium, calcium, and potassium currents. However, the membrane properties of the cell (low R_m) severely limit the spatial extent of the voltage clamp, meaning that there is a potential difference between the soma and distal processes, which in turn generates a significant axial current flow, makes accurate leak subtraction difficult, and yields the current profile with transient and sustained epochs presented here. Because these same properties limit the spatial extent of the voltage clamp, we cannot rule out the presence of voltage-gated channels on fine, distal processes where somatic voltage commands would have little influence on the local membrane potential.

Local dye-coupling was observed in some *Drosophila* astrocytes

The restriction of astrocyte coupling to cells within a hemisegment is reminiscent of findings in the olfactory bulb (Roux et al., 2011) and barrel cortex (Houades et al., 2008), where astrocytes were preferentially coupled within, and not across, anatomo-functional compartments (also reviewed in Giaume and Liu, 2012). We found no difference in the frequency of coupling in channelrhodopsin-stimulated and unstimulated preparations. Isolated larval CNS preparations do vary in their degree of spontaneous, rhythmic activity (Choi et al., 2004; Worrell and Levine, 2008; Berni et al., 2012), and it is plausible that these differences in spontaneous activity across preparations are causally related to the mixed dye-coupling results we obtained. We do not yet know the characteristics of patterns of neuronal activity that might influence changes in glial network connectivity; it is possible that the time course of the ChR2-mediated stimulation protocol we used was insufficient to affect coupling. Nevertheless, the presence of coupling in some preparations strongly suggests that dynamic coupling is present in *Drosophila* astrocytes and establishes that another defining feature of the vertebrate astrocyte is conserved in flies (coupling in mammals: reviewed in Ransom and Giaume, 2013; birds: Kafitz et al., 1999).

Glutamate transporter currents are mediated by *Eaat1*

Tight regulation of glutamate levels in the synaptic space is paramount to brain health across a variety of species; EAATs regulate glutamate-mediated neuroplasticity, protect neurons from excitotoxicity caused by excessive glutamate, and have been implicated in a variety of neurodegenerative and neurological diseases

(Nakagawa and Kaneko, 2013). Much like astrocytes in the rodent hippocampus (Bergles and Jahr, 1997; Meeks and Mennerick, 2007), cerebellum (Clark and Barbour, 1997), cortex (Lalo et al., 2006), spinal cord (Zhang et al., 2009), and brainstem (Huda et al., 2013), *Drosophila* astrocytes show an inward glutamate transporter current in response to neuronal activity. The current is completely blocked by astrocyte-specific expression (alrm-GAL4) of an RNAi hairpin targeting *Eaat1*. In addition to confirming the RNAi target using Eaat1 immunolabeling, we attempted to rescue the looper-evoked astrocyte current by adding a tagged construct (UAS-*Eaat1*-GFP) in addition to the RNAi, but this yielded very little GFP and no significant astrocyte current. Given this cellular phenotype, it is somewhat surprising that the larvae exhibit grossly normal locomotion and development. In contrast, flies carrying null mutations in *Eaat1* do not survive beyond the first-instar larval stage (Stacey et al., 2010), and those with pan–glial-cell RNAi knockdown of *Eaat1* (repo-GAL4) are viable but exhibit a shortened lifespan, neuropil degeneration, and locomotor phenotypes (namely, they can walk but cannot fly; Rival et al., 2004, 2006). This is unexpected given that Eaat1 immunolabeling is localized almost entirely to astrocytes, and alrm-driven RNAi knockdown eliminates any detectable labeling. Presumably, alrm-GAL4–mediated knockdown permits just enough protein production, at the necessary time(s) in embryonic and/or larval development, to allow grossly normal development and locomotor behavior, despite the demonstrated defect in third-instar astrocyte membrane currents.

Spatial relationships that support astrocyte regulation of synaptic signals

Astrocytic processes are found in close proximity to synapses in all brain regions investigated across species, but the degree of contact between astrocytes and synapses varies and is distributed non-uniformly within a region (Bernardinelli et al., 2014). At one extreme, cerebellar synapses formed by climbing fibers in rodents show an average degree of enwrapping around 87% (Xu-Friedman et al., 2001), whereas estimates of degree of enwrapping in the neocortex are lower and suggest that ensheathment is rare ($<$10% of synapses), and contact with the dendritic spine (but not the axon–spine interfaces) dominates (70%) (Genoud et al., 2006). The significance of these differences is poorly understood, but may involve: 1) the stability and maturity of the synapse (Nishida and Okabe, 2007; Medvedev et al., 2014); 2) patterns of neuronal connectivity, such that some areas are by design more disposed to transmitter spillover (Bernardinelli et al., 2014); or 3) dynamic astrocytic process extension and retraction in response to neuronal activity and hormonal changes (Theodosis et al., 2008). These distances, however, should be viewed as relative, as these methods do not account for the actual diffusion pathway, which is tortuous, and all measurements taken from chemically fixed EM preparations are subject to non-uniform shrinkage, making astrocytes appear to be located closer to synapses than they are *in vivo* (Korogod et al., 2015).

As in other species, the spatial relationships between synapses and astrocytic processes in the *Drosophila* larval VNC neuropil are non-uniform, even when the population of presynaptic sites along a single neuron is considered. Our analysis of all 67 presynaptic sites on the selected looper neuron does not offer any examples of complete ensheathment and indicates that direct astrocytic contact with the presynaptic site is rare; however, no synapses were found at a distance greater than 1 μm from an astrocytic process. This upper limit of astrocyte–presynaptic distance ($\sim$1 μm) may represent an important parameter for synapse function.

Although they did not examine the underlying anatomy, results of Liu et al. (2014) in the olfactory pathway of *Drosophila* lend support to the notion that astrocytes regulate synaptic signaling in this species: they overexpressed the TrpA1 channel in astrocytes and found that thermogenetic astrocyte activation modulates excitatory postsynaptic potentials in antennal-lobe projection neurons. The nature of the anatomical relationship between astrocytes and those synapses, however, was not investigated.

The current study clearly demonstrates that neurotransmitter homeostasis and fast regulation of the synaptic signal by transmitter transport are present in the neuropil of the *Drosophila* larval VNC. Our analysis of the same synapse–astrocyte interaction from both an anatomical and physiological perspective demonstrates that astrocytes modulate synaptic communication between looper neurons and motor neurons, despite minimal direct apposition to synaptic elements and a mean separation distance of 0.375 μm between looper presynaptic sites and astrocytic processes. We conclude that even without extensive contact, robust communication between these two cell types is present.

CONCLUSIONS

In conjunction with their previously noted gross anatomical and molecular similarities with astrocytes across the vertebrate phylum, the presence of shared core electrophysiological features in *Drosophila* astrocytes lends strong support to the argument that these

astrocytes are functionally analogous to vertebrate astrocytes. This finding enhances the significance and broad predictive value of mechanistic, molecular-genetic studies of astrocytes in the fly system. Our detailed exploration of the anatomical and physiological interactions between synapses and astrocytic processes demonstrates that astrocytes in *Drosophila* respond to activity at synapses and that glutamate transport by astrocytes affects the postsynaptic response in an anatomical configuration that features no ensheathment and infrequent direct contact. Thus, *Drosophila* gives us an example of a functionally tripartite interaction without a close, classically tripartite, anatomical relationship between synapses and astrocytic processes.

ACKNOWLEDGMENTS

We thank Patricia Jansma for her assistance with all things microscopy; Marvin Landis for extensive guidance on 3D reconstruction; Casey Schneider-Mizell for review of the looper skeleton; Kimberly Lance for skillful lab management; and Emilie Peco and Don van Meyel for kindly sharing reagents prior to publication. We also thank undergraduate lab members Si Woo Lee, Ernesto Hernandez, Leah Kaplan, and Neha Godbole for their skillful assistance throughout this project. SEM gratefully acknowledges the 2012 CSHL *Drosophila* Neurobiology Course (supported by NSF IOS-1238832 and NIDA 1R13DA034437-03) for invaluable training and networking.

CONFLICT OF INTEREST STATEMENT

The authors have no conflicts of interest to disclose.

ROLE OF AUTHORS

All authors had full access to all the data in the study and take responsibility for the integrity of the data and the accuracy of the data analysis. Study concept and design: SEM, LAO. Acquisition of data: SEM, KEL, SG, CTT, RDF, AC. Analysis and interpretation of data: SEM, KEL, CTT. Drafting of the manuscript: SEM. Critical revision of the manuscript for important intellectual content: LAO, LPT, AC. Statistical analysis: SEM. Obtained funding: LAO, LPT, AC. Administrative, technical, and material support: none. Study supervision: LAO, LPT.

DATA ACCESSIBILITY

Data generated in the lab and the subsequent analyses will be made available upon request to the Oland/Tolbert laboratory by qualified individuals as long as doing so would not compromise intellectual property interests or interfere with publication. Any shared data would include notations, standards, and the like that are necessary for interpretation of the data.

LITERATURE CITED

Altenhein B, Becker A, Busold C, Beckmann B, Hoheisel JD, Technau GM. 2006. Expression profiling of glial genes during *Drosophila* embryogenesis. Dev Biol 296:545–560.

Awasaki T, Lai S-L, Ito K, Lee T. 2008. Organization and postembryonic development of glial cells in the adult central brain of *Drosophila*. J Neurosci 28:13742–13753.

Baines RA, Bate M. 1998. Electrophysiological development of central neurons in the *Drosophila* embryo. J Neurosci 18: 4673–4683.

Beckervordersandforth RM, Rickert C, Altenhein B, Technau GM. 2008. Subtypes of glial cells in the Drosophila embryonic ventral nerve cord as related to lineage and gene expression. Mech Dev 125:542–557.

Bergles DE, Jahr CE. 1997. Synaptic activation of glutamate transporters in hippocampal astrocytes. Neuron 19: 1297–1308.

Bernardinelli Y, Muller D, Nikonenko I. 2014. Astrocyte-synapse structural plasticity. Neural Plast 2014:232105.

Berni J, Pulver SR, Griffith LC, Bate M. 2012. Autonomous circuitry for substrate exploration in freely moving *Drosophila* larvae. Curr Biol 22:1861–1870.

Chao T, Rickmann M, Wolff J. 2002. The synapse-astrocyte boundary: an anatomical basis for an integrative role of glia in synaptic transmission. In: The tripartite synapse: glia in synaptic transmission. Volterra A, Magistretti P, Haydon P, editors. New York, NY: Oxford University Press. p 3–23.

Choi JC, Park D, Griffith LC. 2004. Electrophysiological and morphological characterization of identified motor neurons in the Drosophila third instar larva central nervous system. J Neurophysiol 91:2353–2365.

Clark BA, Barbour B. 1997. Currents evoked in Bergmann glial cells by parallel fibre stimulation in rat cerebellar slices. J Physiol 502:335–350.

Coutinho-Budd J, Freeman MR. 2013. Probing the enigma: unraveling glial cell biology in invertebrates. Curr Opin Neurobiol 23:1073–1079.

Cully DF, Paress PS, Liu KK, Schaeffer JM, Arena JP. 1996. Identification of a *Drosophila melanogaster* glutamate-gated chloride channel sensitive to the antiparasitic agent avermectin. J Biol Chem 271:20187–20191.

Dietzl G, Chen D, Schnorrer F, Su K-C, Barinova Y, Fellner M, Gasser B, Kinsey K, Oppel S, Scheiblauer S, Couto A, Marra V, Keleman K, Dickson BJ. 2007. A genome-wide transgenic RNAi library for conditional gene inactivation in *Drosophila*. Nature 448:151–156.

Doherty J, Logan MA, Taşdemir OE, Freeman MR. 2009. Ensheathing glia function as phagocytes in the adult Drosophila brain. J Neurosci 29:4768–4781.

Egger B, Leemans R, Loop T, Kammermeier L, Fan Y, Radimerski T, Strahm MC, Certa U, Reichert H. 2002. Gliogenesis in *Drosophila*: genome-wide analysis of downstream genes of glial cells missing in the embryonic nervous system. Development 129:3295–3309.

Fei H, Chow DM, Chen A, Romero-Calderón R, Ong WS, Ackerson LC, Maidment NT, Simpson JH, Frye MA, Krantz DE. 2010. Mutation of the *Drosophila* vesicular GABA transporter disrupts visual figure detection. J Exp Biol 213:1717–1730.

Fiala JC. 2005. Reconstruct: a free editor for serial section microscopy. J Microsc 218:52–61.

Freeman MR, Delrow J, Kim J, Johnson E, Doe CQ. 2003. Unwrapping glial biology: Gcm target genes regulating glial development, diversification, and function. Neuron 38:567–580.

Genoud C, Quairiaux C, Steiner P, Hirling H, Welker E, Knott GW. 2006. Plasticity of astrocytic coverage and

glutamate transporter expression in adult mouse cortex. PLoS Biol 4:e343.
Giaume C, Liu X. 2012. From a glial syncytium to a more restricted and specific glial networking. J Physiol Paris 106:34–39.
Grenningloh G, Rehm EJ, Goodman CS. 1991. Genetic analysis of growth cone guidance in *Drosophila*: fasciclin II functions as a neuronal recognition molecule. Cell 67:45–57.
Grosche J, Matyash V, Möller T, Verkhratsky A, Reichenbach A, Kettenmann H. 1999. Microdomains for neuron-glia interaction: parallel fiber signaling to Bergmann glial cells. Nat Neurosci 2:139–143.
Grosjean Y, Grillet M, Augustin H, Ferveur J-F, Featherstone DE. 2008. A glial amino-acid transporter controls synapse strength and courtship in *Drosophila*. Nat Neurosci 11:54–61.
Han C, Jan LY, Jan Y-N. 2011. Enhancer-driven membrane markers for analysis of nonautonomous mechanisms reveal neuron-glia interactions in *Drosophila*. Proc Natl Acad Sci U S A 108:9673–9678.
Han X, Chen M, Wang F, Windrem M, Wang S, Shanz S, Xu Q, Oberheim NA, Bekar L, Betstadt S, Silva AJ, Takano T, Goldman SA, Nedergaard M. 2013. Forebrain engraftment by human glial progenitor cells enhances synaptic plasticity and learning in adult mice. Cell Stem Cell 12:342–353.
Hayashi J, Levine RB. 1992. Calcium and potassium current in leg motoneurons during postembryonic development in the hawkmoth *Manduca sexta*. J Exp Biol 171:15–42.
Houades V, Koulakoff A, Ezan P, Seif I, Giaume C. 2008. Gap junction-mediated astrocytic networks in the mouse barrel cortex. J Neurosci 28:5207–5217.
Huda R, McCrimmon DR, Martina M. 2013. pH modulation of glial glutamate transporters regulates synaptic transmission in the nucleus of the solitary tract. J Neurophysiol 110:368–377.
Ito K, Urban J, Technau GM. 1995. Distribution, classification, and development of *Drosophila* glial cells in the late embryonic and early larval ventral nerve cord. Roux's Arch Dev Biol 204:284–307.
Iyengar BG, Chou CJ, Vandamme KM, Klose MK, Zhao X, Akhtar-Danesh N, Campos AR, Atwood HL. 2011. Silencing synaptic communication between random interneurons during *Drosophila* larval locomotion. Genes Brain Behav 10:883–900.
Jan LY, Jan YN. 1976. Properties of the larval neuromuscular junction in *Drosophila melanogaster*. J Physiol 262:189–214.
Kafitz KW, Güttinger HR, Müller CM. 1999. Seasonal changes in astrocytes parallel neuronal plasticity in the song control area HVc of the canary. Glia 27:88–100.
Kafitz KW, Meier SD, Stephan J, Rose CR. 2008. Developmental profile and properties of sulforhodamine 101-labeled glial cells in acute brain slices of rat hippocampus. J Neurosci Methods 169:84–92.
Kimelberg HK, Nedergaard M. 2010. Functions of astrocytes and their potential as therapeutic targets. Neurotherapeutics 7:338–353.
Klapoetke NC, Murata Y, Kim SS, Pulver SR, Birdsey-Benson A, Cho YK, Morimoto TK, Chuong AS, Carpenter EJ, Tian Z, Wang J, Xie Y, Yan Z, Zhang Y, Chow BY, Surek B, Melkonian M, Jayaraman V, Constantine-Paton M, Wong GK-S, Boyden ES. 2014. Independent optical excitation of distinct neural populations. Nat Methods 11:338–346.
Kohsaka H, Takasu E, Morimoto T, Nose A. 2014. A group of segmental premotor interneurons regulates the speed of axial locomotion in *Drosophila* larvae. Curr Biol 24:2632–2642.
Korogod N, Petersen CCH, Knott GW. 2015. Ultrastructural analysis of adult mouse neocortex comparing aldehyde perfusion with cryo fixation. eLife 4:e05793.
Kressin K, Kuprijanova E, Jabs R, Seifert G, Steinhäuser C. 1995. Developmental regulation of Na+ and K+ conductances in glial cells of mouse hippocampal brain slices. Glia 15:173–187.
Kuffler SW, Nicholls JG. 1966. The physiology of neuroglial cells. Ergebnisse Physiol Biol Chem Exp Pharmakol 57:1–90.
Lalo U, Pankratov Y, Kirchhoff F, North RA, Verkhratsky A. 2006. NMDA receptors mediate neuron-to-glia signaling in mouse cortical astrocytes. J Neurosci 26:2673–2683.
Landgraf M, Sánchez-Soriano N, Technau GM, Urban J, Prokop A. 2003. Charting the *Drosophila* neuropile: a strategy for the standardised characterisation of genetically amenable neurites. Dev Biol 260:207–225.
Liu H, Zhou B, Yan W, Lei Z, Zhao X, Zhang K, Guo A. 2014. Astrocyte-like glial cells physiologically regulate olfactory processing through the modification of ORN-PN synaptic strength in *Drosophila*. Eur J Neurosci 40:2744–2754.
Liu WW, Wilson RI. 2013. Glutamate is an inhibitory neurotransmitter in the *Drosophila* olfactory system. Proc Natl Acad Sci U S A 110:10294–10299.
Mahr A, Aberle H. 2006. The expression pattern of the *Drosophila* vesicular glutamate transporter: a marker protein for motoneurons and glutamatergic centers in the brain. Gene Expr Patterns 6:299–309.
Marley R, Baines RA. 2011. Whole-cell patch recording from *Drosophila* larval neurons. Cold Spring Harb Protoc 2011. DOI: 10.1101/pdb.prot065664.
Mathew D, Popescu A, Budnik V. 2003. *Drosophila* amphiphysin functions during synaptic Fasciclin II membrane cycling. J Neurosci 23:10710–10716.
Matthias K, Kirchhoff F, Seifert G, Huttmann K, Matyash M, Kettenmann H, Steinhauser C. 2003. Segregated expression of AMPA-type glutamate receptors and glutamate transporters defines distinct astrocyte populations in the mouse hippocampus. J Neurosci 23:1750–1758.
Matyash V, Kettenmann H. 2010. Heterogeneity in astrocyte morphology and physiology. Brain Res Rev 63:2–10.
Medvedev N, Popov V, Henneberger C, Kraev I, Rusakov DA, Stewart MG. 2014. Glia selectively approach synapses on thin dendritic spines. Philos Trans R Soc Lond B Biol Sci 369:20140047.
Meeks JP, Mennerick S. 2007. Astrocyte membrane responses and potassium accumulation during neuronal activity. Hippocampus 17:1100–1108.
Mezler M, Muller T, Raming K. 2001. Cloning and functional expression of GABAB receptors from *Drosophila*. Eur J Neurosci 13:477–486.
Muthukumar AK, Stork T, Freeman MR. 2014. Activity-dependent regulation of astrocyte GAT levels during synaptogenesis. Nat Neurosci 17:1340–1350.
Nakagawa T, Kaneko S. 2013. SLC1 glutamate transporters and diseases: psychiatric diseases and pathological pain. Curr Mol Pharmacol 6:66–73.
Ng FS, Tangredi MM, Jackson FR. 2011. Glial cells physiologically modulate clock neurons and circadian behavior in a calcium-dependent manner. Curr Biol 21:625–634.
Nishida H, Okabe S. 2007. Direct astrocytic contacts regulate local maturation of dendritic spines. J Neurosci 27:331–340.
Oberheim NA, Goldman SA, Nedergaard M. 2012. Heterogeneity of astrocytic form and function. In: Astrocytes. Milner R, editor. Vol. 814. Totowa, NJ: Humana Press. p 23–45.
Ohyama T, Schneider-Mizell CM, Fetter RD, Aleman JV, Franconville R, Rivera-Alba M, Mensh BD, Branson KM, Simpson JH, Truman JW, Cardona A, Zlatic M. 2015. A

multilevel multimodal circuit enhances action selection in *Drosophila*. Nature 520:633–639.

Peco E, Davla S, Camp D, Stacey S, Landgraf M, van Meyel D. 2016. *Drosophila* astrocytes cover specific territories of CNS neuropil and are instructed to differentiate by Prospero, a key effector of Notch. Development 143: 1170–1181.

Pfeiffer BD, Ngo TT, Hibbard KL, Murphy C, Jenett A, Truman JW, Rubin GM. 2010. Refinement of tools for targeted gene expression in *Drosophila*. Genetics 186:735–755.

Pulver SR, Pashkovski SL, Hornstein NJ, Garrity PA, Griffith LC. 2009. Temporal dynamics of neuronal activation by Channelrhodopsin-2 and TRPA1 determine behavioral output in *Drosophila* larvae. J Neurophysiol 101:3075–88.

Ramachandran P, Budnik V. 2010. Embryonic and larval neuromuscular junction. Drosophila neurobiology: a laboratory manual. In: Zhang B, Freeman MR, Waddell S, editors. 1st ed. Cold Spring Harbor, NY: Cold Spring Harbor Laboratory Press. p 93–123.

Ransom BR, Giaume C. 2013. Gap junction and hemichannels. In: Neuroglia. Kettenmann H, Ransom BR, editors. 3rd ed. New York, NY: Oxford University Press. p 292–305.

Rival T, Soustelle L, Strambi C, Besson M-T, Iché M, Birman S. 2004. Decreasing glutamate buffering capacity triggers oxidative stress and neuropil degeneration in the *Drosophila* brain. Curr Biol 14:599–605.

Rival T, Soustelle L, Cattaert D, Strambi C, Iché M, Birman S. 2006. Physiological requirement for the glutamate transporter dEAAT1 at the adult *Drosophila* neuromuscular junction. J Neurobiol 66:1061–1074.

Rohrbough J, Broadie K. 2002. Electrophysiological analysis of synaptic transmission in central neurons of *Drosophila* larvae. J Neurophysiol 88:847–860.

Roux L, Benchenane K, Rothstein JD, Bonvento G, Giaume C. 2011. Plasticity of astroglial networks in olfactory glomeruli. Proc Natl Acad Sci U S A 108:18442–18446.

Saalfeld S, Cardona A, Hartenstein V, Tomancak P. 2009. CATMAID: collaborative annotation toolkit for massive amounts of image data. Bioinformatics 25:1984–1986.

Schneider-Mizell CM, Gerhard S, Longair M, Kazimiers T, Li F, Zwart MF, Champion A, Midgley F, Fetter R, Saalfeld S, Cardona A. 2016. Quantitative neuroanatomy for connectomics in *Drosophila*. eLIFE 5:e12059.

Schools GP, Zhou M, Kimelberg HK. 2006. Development of gap junctions in hippocampal astrocytes: evidence that whole cell electrophysiological phenotype is an intrinsic property of the individual cell. J Neurophysiol 96:1383–1392.

Schroder W, Hinterkeuser S, Seifert G, Schramm J, Jabs R, Wilkin GP, Steinhauser C. 2000. Functional and molecular properties of human astrocytes in acute hippocampal slices obtained from patients with temporal lobe epilepsy. Epilepsia 41:S181–S184.

Shimamoto K, LeBrun B, Yasuda-Kamatani Y, Sakaitani M, Shigeri Y. 1998. A potent blocker of excitatory amino acid transporters. Mol Pharmacol 201:195–201.

Stacey SM, Muraro NI, Peco E, Labbé A, Thomas GB, Baines RA, van Meyel DJ. 2010. *Drosophila* glial glutamate transporter Eaat1 is regulated by fringe-mediated notch signaling and is essential for larval locomotion. J Neurosci 30:14446–14457.

Stebbings LA, Todman MG, Phillips R, Greer CE, Tam J, Phelan P, Jacobs K, Bacon JP, Davies JA. 2002. Gap junctions in *Drosophila*: developmental expression of the entire innexin gene family. Mech Dev 113:197–205.

Steinhäuser C, Kressin K, Kuprijanova E, Weber M, Seifert G. 1994. Properties of voltage-activated Na+ and K+ currents in mouse hippocampal glial cells in situ and after acute isolation from tissue slices. Pflugers Arch 428: 610–620.

Stork T, Sheehan A, Tasdemir-Yilmaz OE, Freeman MR. 2014. Neuron-glia interactions through the Heartless FGF receptor signaling pathway mediate morphogenesis of *Drosophila* Astrocytes. Neuron 83:388–403.

Takagawa K, Salvaterra P. 1996. Analysis of choline acetyltransferase protein in temperature sensitive mutant flies using newly generated monoclonal antibody. Neurosci Res 24:237–243.

Theodosis DT, Poulain DA, Oliet SHR. 2008. Activity-dependent structural and functional plasticity of astrocyte-neuron interactions. Physiol Rev 88:983–1008.

Thimgan MS, Berg JS, Stuart AE. 2006. Comparative sequence analysis and tissue localization of members of the SLC6 family of transporters in adult *Drosophila melanogaster*. J Exp Biol 209:3383–3404.

Uwechue NM, Marx M-C, Chevy Q, Billups B. 2012. Activation of glutamate transport evokes rapid glutamine release from perisynaptic astrocytes. J Physiol 590:2317–2331.

Vassilatis DK, Elliston KO, Paress PS, Hamelin M, Arena JP, Schaeffer JM, Van der Ploeg LH, Cully DF. 1997. Evolutionary relationship of the ligand-gated ion channels and the avermectin-sensitive, glutamate-gated chloride channels. J Mol Evol 44:501–508.

Venken KJT, Simpson JH, Bellen HJ. 2011. Genetic manipulation of genes and cells in the nervous system of the fruit fly. Neuron 72:202–230.

Verkhratsky A, Butt AM. 2013. Glial physiology and pathophysiology. Hoboken, NJ: Wiley-Blackwell.

Verkhratsky A, Nedergaard M. 2014. Astroglial cradle in the life of the synapse. Philos Trans R Soc B Biol Sci 369: 20130595.

Wolstenholme AJ. 2012. Glutamate-gated chloride channels. J Biol Chem 287:40232–40238.

Worrell JW, Levine RB. 2008. Characterization of voltage-dependent Ca^{2+} currents in identified *Drosophila* motoneurons in situ. J Neurophysiol 100:868–878.

Xu-Friedman MA, Harris KM, Regehr WG. 2001. Three-dimensional comparison of ultrastructural characteristics at depressing and facilitating synapses onto cerebellar Purkinje cells. J Neurosci 21:6666–6672.

Yamazaki D, Horiuchi J, Ueno K, Ueno T, Saeki S, Matsuno M, Naganos S, Miyashita T, Hirano Y, Nishikawa H, Taoka M, Yamauchi Y, Isobe T, Honda Y, Kodama T, Masuda T, Saitoe M. 2014. Glial dysfunction causes age-related memory impairment in *Drosophila*. Neuron 84:753–763.

Yeh E, Gustafson K, Boulianne GL. 1995. Green fluorescent protein as a vital marker and reporter of gene expression in *Drosophila*. Proc Natl Acad Sci U S A 92:7036–7040.

Zayas-Santiago A, Agte S, Rivera Y, Benedikt J, Ulbricht E, Karl A, Dávila J, Savvinov A, Kucheryavykh Y, Inyushin M, Cubano LA, Pannicke T, Veh RW, Francke M, Verkhratsky A, Eaton MJ, Reichenbach A, Skatchkov SN. 2014. Unidirectional photoreceptor-to-Müller glia coupling and unique K+ channel expression in Caiman retina. PLoS One 9:e97155.

Zhang H, Xin W, Dougherty PM. 2009. Synaptically evoked glutamate transporter currents in spinal dorsal horn astrocytes. Mol Pain 5:36.

Zhou M, Kimelberg HK. 2000. Freshly isolated astrocytes from rat hippocampus show two distinct current patterns and different $[K^+]_o$ uptake capabilities. J Neurophysiol 84: 2746–2757.

Zhou M, Kimelberg HK. 2001. Freshly isolated hippocampal ca1 astrocytes comprise two populations differing in glutamate transporter and AMPA receptor expression. J Neurosci 21:7901–7908.